Trypanosoma cruzi possess the cysteine biosynthetic pathway. *E. histolytica* is the enteric protozoan parasite that causes amoebic colitis and extra intestinal abscesses (hepatic, pulmonary and cerebral) in inhabitants of endemic areas and is estimated to cause severe disease in 48 million people, killing about 70,000 each year [15]. While *E. histolytica* synthesizes L-cysteine via sulfur assimilatory pathway like plants and bacteria, it lacks, based on the genome information, both forward and reverse trans-sulfuration pathways [16,17], which makes this organism, together with *T. vaginalis*, very unique. In this organism, L-cysteine is essential for the synthesis of various proteins and the Fe–S cluster of Fe–S proteins such as ferredoxin and pyruvate:ferredoxin oxidoreductase. L-Cysteine has also been shown to be necessary for growth, survival, attachment, and anti-oxidation in this parasite [17,18].

The recent disclosure of the whole genome [19] revealed that *E. histolytica* possesses three isoenzymes each of CS and SAT [18,20]. We previously demonstrated the biochemical features of two CS isoforms (EhCS1and EhCS2) [16,21], and one SAT isoform, EhSAT1 hereinafter, [17]. In the present study, we biochemically characterized the two remaining SAT isotypes (EhSAT2 and EhSAT3), and compared kinetic parameters as well as their feedback-regulatory mechanisms.

2. Materials and methods

2.1. Chemicals

Acetyl-CoA, L-serine, Na_2S, glucose, ninhydrin reagent, trans-epoxysuccinyl-L-leucylamido-(4-guanidino) butane (E-64) were purchased from Sigma–Aldrich (Tokyo, Japan). All other chemicals of analytical grade were purchased from Wako (Tokyo, Japan) unless otherwise stated.

2.2. Microorganisms and cultivation

Trophozoites of the *E. histolytica* clonal strain HM1: IMSS cl 6 were maintained axenically in Diamond's BI-S-33 medium at 35.5 °C as described previously [22,23]. Trophozoites were harvested in the late-logarithmic growth phase for 2–3 days after inoculation of one-thirtieth to one-twelfth of the total culture volume. After the cultures were chilled on ice for 5 min, trophozoites were collected by centrifugation at 500 × *g* for 10 min at 4 °C and washed twice with ice-cold PBS, pH 7.4. *Escherichia coli* BL21 (DE3) pLysS strain was purchased from Invitrogen (Tokyo, Japan).

2.3. Construction of plasmids

Standard techniques were used for cloning and plasmid construction as previously described [24]. Genes encoding *E. histolytica* SAT1, SAT2, and SAT3 (EhSAT1-3) were cloned to produce a fusion protein containing a histidine-tag (provided by the vector) at the amino terminus. The cDNA corresponding to an open reading frame of EhSAT1-3 of 305, 311, and 336 amino acid residues with a calculated molecular mass of 34.4, 34.8, and 37.7 kDa, respectively, were amplified by PCR using the *E. histolytica* cDNA library [16] as a template and oligonucleotide primers. The sense and antisense oligonucleotide primers used for EhSAT1, EhSAT2 and EhSAT3 were: 5′-CCT**GGATCC**GATGGACAATTACATTTATTCAATTGCACAT-3′ and 5′-CCA**GGATCC**TTAAATCGATGGTGAATTTGCTAAAGGAGAT-3′ (EhSAT1); 5′-CCT**GGATCC**GATGGATTTACTTGTTTCAAAAATTTCAAAA-3′ and 5′-CCA**GGATCC**CTAATTTAAAGGAGAGTTTATTGGACTTATT-3′ (EhSAT2); 5′-CCT**GGATCC**GATGAGTTCTTTACTACAACAAACATCTCAG-3′ and 5′-CCA**GGATCC**TTATTGTTGACAAGATACAAAACAATCTAA-3′ (EhSAT3), respectively, where bold letters indicate BamHI restriction sites. PCR was performed with platinum pfx DNA polymerase (Invitrogen) and the following parameters: an initial incubation at 94 °C for 2 min; followed by the 30 cycles of denaturation at 94 °C for 15 s, annealing at 50, 45, or 55 °C for EhSAT1-3, respectively, for 30 s, and elongation at 68 °C for 1 min, and a final extension at 68 °C for 10 min. The PCR fragment was digested with BamHI and electrophoresed, purified with Gene clean kit II (BIO 101, Vista, CA, USA), and ligated into BamHI-digested pET-15b (Novagen, Darmstadt, Germany) in the same orientation as the T7 promoter to produce pET-EhSAT1, pET-EhSAT2 and pET-EhSAT3. The nucleotide sequences of the cloned EhSAT1, EhSAT2, and EhSAT3 were verified by sequencing to be identical to the putative protein coding region of 200.m00078, 253.m00083, and 13.m00319, respectively.

2.4. Bacterial expression and purification of recombinant E. histolytica SAT isotypes

The above mentioned plasmids were introduced into *E. coli* BL21 (DE3) pLysS cells by heat shock at 42 °C for 1 min. *E. coli* BL21 (DE3) harboring pET-EhSAT1, pET-EhSAT2 or pET-EhSAT3 were grown at 37 °C in 100 ml of Luria Bertani (LB) medium in the presence of 100 μg/ml ampicillin. The overnight culture was used to inoculate 500 ml of fresh medium, and the culture was further continued at 37 °C with shaking at 180 rpm. When A_{600} reached 0.6, 0.4 mM of isopropyl β-D-thio galactopyranoside (IPTG) was added, and cultivation was continued for another 4 h at 30 °C. *E. coli* cells from the induced culture were harvested by centrifugation at 4050 × *g* for 20 min at 4 °C. The cell pellet was washed with PBS, pH 7.4, re-suspended in 15 ml of the lysis buffer (50 mM Tris–HCl, pH 8.0, 300 mM NaCl, and 10 mM imidazole) containing 0.1% Triton X-100 (v/v), 100 μg/ml lysozyme and 1 mM phenylmethyl sulfonyl fluoride (PMSF) incubated at room temperature for 30 min, sonicated on ice and centrifuged at 25,000 × *g* for 15 min at 4 °C. The supernatant was mixed with 2 ml of 50% Ni^{2+}-NTA His-bind slurry, incubated for 2 h at 4 °C with mild shaking. The recombinant EhSAT (rEhSAT)-bound resin in a column was washed three times each with buffer A [50 mM Tris–HCl, pH 8.0, 300 mM NaCl, and 0.1% Triton X-100, v/v] containing 10–50 mM of imidazole. Bound proteins were eluted with buffer A containing 100–300 mM imidazole.

After the integrity and the purity of rEhSAT proteins were confirmed with 12% SDS-PAGE analysis, followed by Coomassie Brilliant Blue staining, they were extensively dialyzed twice against the 300-fold volume of 50 mM Tris–HCl, 150 mM NaCl, pH 8.0 containing 10% glycerol (v/v) and the Complete Mini protease inhibitor cocktail (Roche, Mannheim, Germany) for 18 h at 4 °C. The dialyzed proteins were stored at −80 °C with 20% glycerol in small aliquots until further use. The purified proteins remained fully active after >3 months under these conditions. Protein concentrations were spectrophotometrically determined by Bradford method using BSA as a standard as previously described [25].

2.5. Kinetic studies of recombinant SAT isotypes

The SAT activity was determined by two methods, by either monitoring the decrease in A_{232} due to the cleavage of the thioester bond of acetyl-CoA [26] or the coupling reaction with CS [27], followed by the colorimetric ninhydrin assay. For the thioester-bond cleavage assay, the standard mixture contained 50 mM Tris–HCl (pH 8.0), 0.1 mM acetyl-CoA, 1 mM L-serine and 2.5 μg of rEhSAT. The reaction was initiated by the addition of L-serine and carried out at 25 °C for 3–5 min. The decrease in absorbance at 232 nm was

monitored on a spectrophotometer (Shimadzu, UV 2550) equipped with an automatic cell changer. The K_m and V_{max} values were estimated with Hanes–Woolf and Line weaver–Burk plots. Kinetic studies were performed using 5–7 concentrations of both acetyl Co-A and L-serine. All steady-state kinetic parameters are the means of three to five independent experiments where two or three different preparations of recombinant SATs were used for measurements performed on at least three non-consecutive days. The coupling reaction was used only when SAT activity of the recombinant enzymes was initially demonstrated. The standard assay mixture contained 50 mM Tris–HCl (pH 8.0), 0.4 mM acetyl-CoA, 4 mM L-serine, 5 mM Na_2S, 10 mM DTT, 0.5 μg of recombinant EhCS3 and 2.5 μg of rEhSAT, in a final volume of 100 μl. The reaction was performed at 37 °C for 15–30 min, and the amount of L-cysteine was determined as described [28].

2.6. Amino acid comparison and phylogenetic analysis

Amino acid sequences of SAT from 48 other organisms that showed significant similarity to EhSATs were obtained from the DDBJ/EBI/GenBank database by using blastp search. Sequence alignments of these proteins were generated using CLUSTAL W program [29]. The alignment obtained by CLUSTAL W was inspected and manually corrected using Genedoc program (www.psc.edu/biomed/genedoc). All gaps were removed and unambiguously aligned 245 conserved sites were selected and used for phylogenetic analyses. The neighbor-joining (NJ) and maximum parsimony (MP) methods were performed using MEGA4 program [30]. A final phylogenetic tree of 35 sequences was drawn by using MEGA4. The branch lengths in these trees were obtained from the neighbor-joining analysis with bootstrap values in 100 replicates.

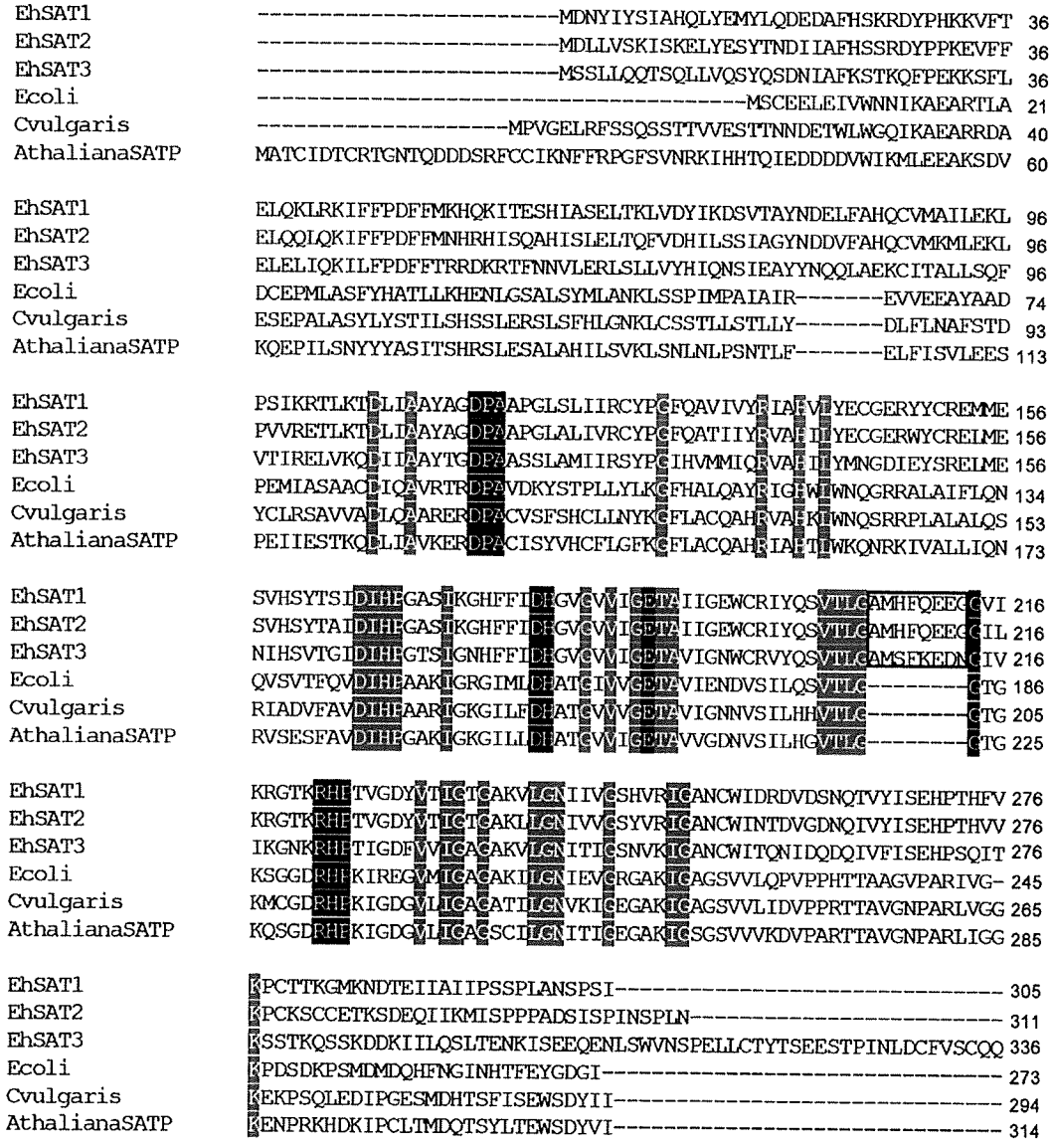

Fig. 1. Complete protein sequences of *E. histolytica* and other organisms were aligned using the CLUSTAL W program (http://clustalw.ddbj.nig.ac.jp/top-e.html). Accession numbers of these sequences are: *Escherichia coli* (NP415427), *Citrullus vulgaris* (D85624), *Arabidopsis thaliana SAT-p* (Q42538), *E. histolytica EhSAT1-3* (AB023954, AB232374 and AB232375). *Dashes* indicate gaps. Highly conserved residues that were shown to participate in the binding to substrates (acetyl-CoA and L-serine) and L-cysteine based on crystal structures of *E. coli* SAT [31,32] are highlighted in *black*. Other amino acids conserved among these organisms are highlighted in *grey*. An insertion unique to the amoebic SATs is *boxed*.

3. Results

3.1. Identification of genes and their encoded proteins of three SAT isotypes from E. histolytica

We identified genes encoding three SAT isotypes by homology search against the *E. histolytica* genome database [19] using SAT protein sequences from bacteria, yeast, and plants. We designated them as *EhSAT1*, *EhSAT2*, and *EhSAT3* genes [corresponding to 200.m00078 (AB023954, XM_645673 and XP_650765) [17], 253.m00083 (AB232374, XM_644909 and XP_650001), and 13.m00319 (AB232375, XM_651281 and XP_656373), respectively]. *EhSAT1*, *EhSAT2*, or *EhSAT3* gene contains a 918, 936, or 1011-bp open reading frame which encodes the protein of 305, 311, or 336 amino acid residues with a predicted molecular mass of 34.4, 34.8, or 37.7 kDa and p*I* of 6.63, 5.99, or 5.70, respectively.

3.2. Features of the deduced amino acid sequences of E. histolytica SATs

The amino acid sequence of EhSATs showed 21–42% identities to SAT from archaea, bacteria, and plants. SAT from the square archaeon *Haloquadratum walsbyi* showed the highest (39–42%) amino acid identities to EhSATs. The identity to SAT from other organisms was significantly lower than *H. walsbyi* SAT. For instance, EhSAT3 showed only 27, 24, or 19% identity to *E. coli SAT*, watermelon SAT-c, or *A. thaliana* SAT-p, respectively. The identity between EhSAT1 and EhSAT2, between EhSAT1 and EhSAT3, or between EhSAT2 and EhSAT3 was 73%, 48%, or 48%, respectively. All EhSATs were devoid of the amino-terminal transit peptide found in plastid or mitochondria-located SAT from plants [26,27], which suggests that amoebic SAT genes encode cytosolic proteins. Multiple alignment of 48 SAT sequences was produced by Clustal W, and comparison of only representative SAT sequences from *E. coli*,

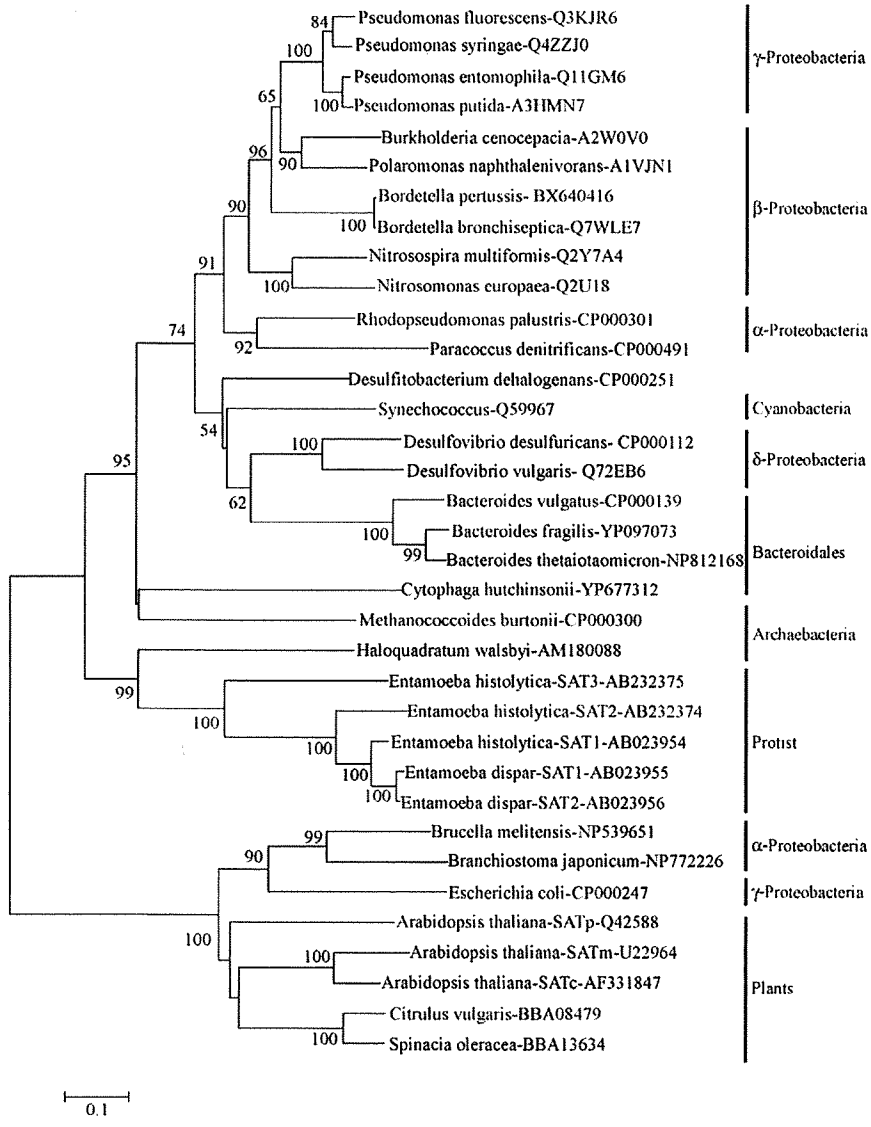

Fig. 2. Phylogenetic reconstruction of SAT proteins from a variety of organisms. A phylogenetic tree of 35 SAT proteins was constructed by using CLUSTAL W program and drawn with MEGA4 program. The number at the nodes represents the bootstrap value in percentage of 1000 replicates. The scale bar indicates 0.1 substitutions at each amino acid position. Species names and accession numbers of the sequences are also indicated.

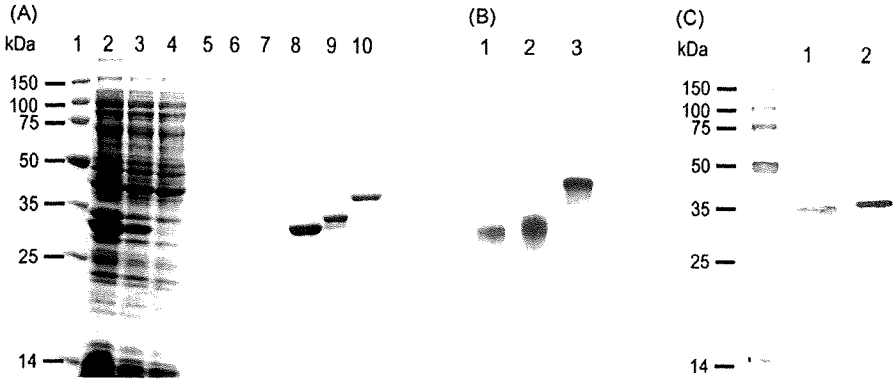

Fig. 3. Expression and purification of the recombinant EhSATs and detection of native EhSATs in the parasite lysate. (A) The *Escherichia coli* BL21 (DE3) strain was transformed with pET-EhSAT1, pET-EhSAT2, and pET-EhSAT3. The recombinant EhSAT1-3 protein was purified on a Ni^{2+}-NTA agarose column. Proteins at each step of purification were resolved on a 12.5% SDS-PAGE gel and stained with Coomassie Brilliant Blue. Lane 1, Molecular weight markers; lanes 2–4, the total lysate (2), supernatant fraction (3), or unbound fraction (4) of the IPTG-induced culture of the pET-EhSAT1-transformed cells; lanes 5–7, fractions eluted with 10, 20, and 50 mM imidazole, respectively; lanes 8–10, purified recombinant EhSAT1, EhSAT2, and EhSAT3, respectively, eluted with 200 mM imidazole. (B) Silver staining of the purified EhSAT1-3 (lanes 1–3, respectively). (C) Immunoblot analysis of the fractionated amebic lysate with anti-EhSAT1 and anti-EhSAT2 antibodies. A fraction eluted from a Mono Q anionic exchange chromatograph was electrophoresed, blotted, and reacted with 200× diluted anti-EhSAT1 (lane 1) or anti-EhSAT2 antibody (lane 2), followed by the reaction with the secondary antibody.

cytosolic SAT from watermelon, and plastid SAT from *A. thaliana* are shown to highlight important similarities and differences among SAT proteins from these organisms and between EhSAT isotypes (Fig. 1).

All the important residues implicated in the active site of the catalytic domain [31] are well conserved in EhSATs. For instance, the residues of Asp-114, Pro-115, Ala-116, Asp-179, and His-180 of EhSAT1, corresponding to Asp-92, Pro-93, Ala-94, Asp-157, and His-158, respectively, of *E. coli* SAT are well conserved. In contrast, there are also notable peculiarities of the amoebic SAT. First, *E. histolytica* SATs have a unique insertion between the coils 2 and 3 of the extended loop of LβH (a.a. 206–213 of EhSAT1-3, corresponding to between a.a. 183 and 184 of *E. coli* SAT). Interestingly, this insertion is also uniquely, other than in *Entamoeba*, present in *H. walsbyi*. Second, Thr-185 of *E. coli* SAT, which is responsible for the interaction with the carboxyl terminus of another subunit of a SAT trimer upon conformational changes caused by the L-cysteine attachment and subsequent in-sensitization of the enzyme to acetyl-CoA [32], is not conserved in amoebic SATs; this residue is substituted with Val or Ile in EhSAT1-3. Third, Ala-218 of *E. coli* SAT, which is involved in the hydrogen bonding with the carbonyl group of cofactor pantetheinyl moiety and the stabilization of CoA in the cleft between two subunits of the trimer [32], is substituted with Val-248 in all three amoebic SATs. Fourth, the amino acid residues around Met-256 of *E. coli* or Met-280 from watermelon have been implicated in the in-sensitivity to L-cysteine. For instance, the Gly-277 to Cys substitution caused in-sensitivity of watermelon SAT to L-cysteine. However, none of the residues in this region is conserved in EhSATs.

There are also isotype-specific features among EhSATs. In particular, EhSAT3 is significantly divergent. First, the amoeba-specific block insertion (a.a. 206–213) found in EhSAT1, EhSAT2, and two SATs from non-pathogenic *Entamoeba dispar* (data not shown) is not shared by EhSAT3. Second, EhSAT3 possesses a 26-a.a. carboxyl-terminal extension, similar to one in the cytosolic *A. thaliana* SAT, which is not shared by other amoebic SATs. Third, although Ile-314 of *A. thaliana* SAT-p and in other organisms (*E. coli* or *H. influenza*), which is necessary for the complex formation with CS [33], is conserved in EhSAT1(Ile-305), it is not conserved in EhSAT2 and EhSAT3.

3.3. Phylogenetic analysis

Phylogenetic reconstruction was performed by NJ and MP programs using 35 SAT protein sequences from various organisms. The NJ tree (Fig. 2) demonstrates three major monophylic groups of SAT: the first group consisting of α-, β-, γ-, and δ-proteobacteria, cyanobacteria, *Bacteriodes*, and one archaeon organism, *Methanococcoides burtonii*, the second consisting of *Entamoeba* and *H. walsbyi*, and the third consisting of plants and a few bacteria belonging to α- and γ-proteobacteria. The high homology, the common amino acid insertion, and the phylogenetic relationship between SAT from *Entamoeba* and *H. walsbyi* suggest that *E. histolytica* most likely obtained a SAT gene from the ancestral organism of *H. walsbyi* by lateral gene transfer, similar to a number of metabolism enzymes [19,20,34]. Phylogenetic reconstruction using MP method also supports the above-mentioned conclusion (data not shown).

3.4. Expression and purification of recombinant EhSAT isotypes

The recombinant EhSATs were overproduced at the level of 20–25% of the soluble proteins in *E. coli* BL21 cells. 12% SDS-PAGE followed by Coomassie Brilliant Blue staining of the purified rEhSAT proteins showed that the rEhSAT1-3 was present as a single

Table 1
Kinetic parameters of EhSAT1, EhSAT2, and EhSAT3.

	L-Serine			Acetyl-CoA		
	K_m (mM)	V_{max} (μmol/min/mg)	k_{cat} (s)	K_m (mM)	V_{max} (μmol/min/mg)	k_{cat} (s)
Eh SAT1	0.12 ± 0.03	41.39 ± 1.43	25.52 ± 0.89	0.55 ± 0.20	95.10 ± 2.50	58.63 ± 2.67
Eh SAT2	0.09 ± 0.02	27.77 ± 1.57	17.31 ± 0.98	0.25 ± 0.02	23.42 ± 0.90	14.59 ± 0.56
Eh SAT3	0.10 ± 0.04	65.75 ± 3.15	43.83 ± 0.90	0.20 ± 0.07	176.83 ± 11.72	117.89 ± 7.81

Note: All reactions were performed as described under "Experimental procedures". All values are expressed as a mean ± S.E. of triplicates.

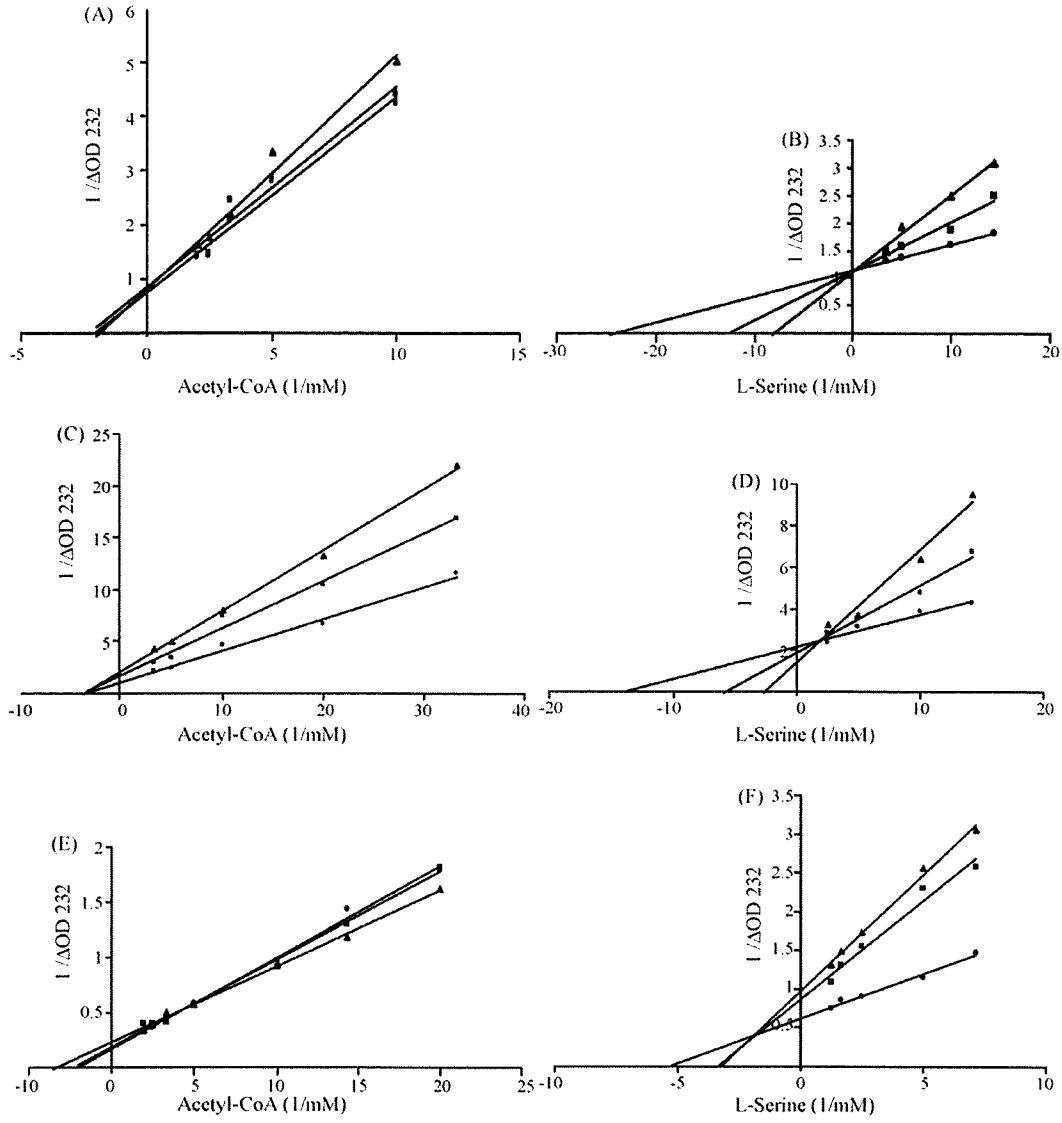

Fig. 4. Double-reciprocal plots of the recombinant EhSATs. The enzymatic activities of EhSAT1 (A and B), EhSAT2 (C and D), and EhSAT3 (E and F) were determined at various concentrations of acetyl-CoA (A, C, and E) and L-serine (B, D, and F) in the presence or absence of L-cysteine. Kinetic studies were performed by monitoring the decrease in A_{232} with a fixed concentration of 0.5 mM L-serine (A, C, and E) and 0.25 mM acetyl-CoA (B, D, and F). Data are shown in the mean of triplicate analyses. (A and B) Symbols are: ●, without L-cysteine; ■, in the presence of 5 μM L-cysteine; and ▲, 10 μM L-cysteine. (C and D) ●, without L-cysteine; ■, in the presence of 50 μM L-cysteine; and ▲, 100 μM L-cysteine. (E and F) ●, without L-cysteine; ■, in the presence of 0.5 mM L-cysteine; and ▲, 1 mM L-cysteine.

homogenous band corresponding to 37.0, 37.4, or 40.0 kDa, respectively, under reducing conditions (Fig. 3). The mobility of rEhSAT1-3 was consistent with the predicted size of the monomeric EhSAT proteins with an extra 2.6 kDa histidine tag added at the amino terminus. The purity of rEhSATs was estimated more than 95% as judged by densitometric scanning of the stained gel. EhSAT proteins were stable and retained their full activity when stored with 10–15% glycerol at −30 or −80 °C for at least 3 months. These purified EhSAT proteins showed no CS activity, suggesting that there is no interaction with *E. coli* CS (CysK and CysM) (data not shown).

3.5. Catalytic and regulatory properties of recombinant EhSATs

Since the purified recombinant EhSATs were free of bacterial CS, the catalytic and regulatory properties of these proteins could be examined without any influence of bacterial CS, which might otherwise potentially activates SAT. The kinetic parameters of rEhSAT1 determined in this study (Table 1) were consistent with those reported previously [17]. The K_m, the V_{max}, and the k_{cat} of three EhSAT proteins slightly varied, but were comparable.

The effects of L-cysteine on the activity of recombinant EhSATs were examined (Fig. 4A–F and Table 2). The inhibition of EhSAT by L-cysteine was isotype specific. The activity of EhSAT1 was inhibited by micromolar concentrations of L-cysteine. Double reciprocal plots in the presence or absence of 5 or 10 μM of L-cysteine, showed that the EhSAT1 activity was inhibited by L-cysteine in a competitive manner with L-serine, but no any significant inhibition was observed in case of acetyl-CoA in the presence of 0.25 mM of acetyl-CoA or 0.5 mM of L-serine (Fig. 4A and B and Table 2). EhSAT2 showed in-sensitivity to these concentrations (5 or 10 μM) of L-cysteine. Approximately 10-fold higher concentrations, i.e., 50–100 μM, of L-cysteine were needed to cause inhibition of EhSAT2 activity comparable to that of EhSAT1. Double reciprocal plots showed that the EhSAT2 activity was inhibited by L-cysteine

Table 2
Inhibition constants (K_i) of recombinant *E. histolytica* SATs by L-cysteine.

	K_i (μM)		
	L-Serine	Acetyl-CoA	Sensitivity
EhSAT1	4.7 ([b]competitive)	[a]–	Sensitive
EhSAT2	27.79 ([b]competitive)	94.7 ([b]non-competitive)	Intermediate
EhSAT3	460 ([b]mix)	[a]–	Insensitive

The enzymatic activities were determined in vitro as described under section 2. To determine the K_i value for L-serine or acetyl-CoA, the constant concentration of acetyl-CoA (0.25 mM) or L-serine (0.5 mM) was used. All values are expressed as a mean ± S.E. of triplicates.

[a] No inhibition by L-cysteine.

[b] The mode of inhibition is shown in parenthesis.

Table 3
Inhibition of EhSATs by structurally related compounds.

Compounds	Concentrations (mM)	Inhibition (%)		
		EhSAT1	EhSAT2	EhSAT3
L-Cysteine	0.03	97.3	<0.5	<0.5
L-Cysteine	0.5	95.4	75.3	<0.5
L-Cysteine	1	98.5	ND	37.8
L-Cystine	0.03	3.6	0.9	7.9
D-Cysteine	0.5	2.2	3.9	4.8
DL-Homocysteine	0.5	7.7	0.9	8.7
DL-Homoserine	0.5	7.7	8.8	5.5
N-Acetyl-L-cysteine	1	25	13.3	27.8
N-Acetyl-L-serine	0.5	11.8	4.9	7.9
Glutathione (oxidized)	0.5	1.3	0.9	19.9
Glutathione (reduced)	0.5	ND	10.3	10.7

ND, Not determined.

in a competitive manner with L-serine and in a non-competitive manner with acetyl-CoA (Fig. 4C and D and Table 2). The K_i value of EhSAT2 by L-cysteine was about 6-fold higher than that of EhSAT1.

In contrast, EhSAT3 was totally in-sensitive to L-cysteine at the concentrations that abolished EhSAT1 and EhSAT2 activity, and very high concentrations of L-cysteine (0.5 or 1 mM) were required to inhibit EhSAT3 activity. At these L-cysteine concentrations, the pattern of inhibition was in a mixed manner with L-serine, but no inhibition was seen for acetyl-CoA (Fig. 4E and F and Table 2). The K_i value of EhSAT3 by L-cysteine was 98 or 18-fold higher than that of EhSAT1 or EhSAT2, respectively.

3.6. Inhibition of EhSAT activity by compounds structurally related to L-cysteine

L-Cysteine showed significant inhibition of EhSAT1 at 30 μM (97%), when 0.5 mM L-serine and 0.2 mM of acetyl-CoA were used. Under the identical conditions, only weak inhibition was observed at 30 μM of L-cystine (<4%), which is contradictory to our previous report [17], but in accordance with other reports on SAT from plants and bacteria. This contradiction might be due to the new expression protocol and the far better purity of EhSAT1 obtained in the present study. Other compounds showed no inhibition against EhSAT1 except for N-acetyl-L-serine and N-acetyl-L-cysteine (Table 3). EhSAT2 was inhibited with 0.5 mM L-cysteine by 75%, while N-acetyl-L-cysteine and reduced glutathione showed marginal inhibition. Inhibition of EhSAT3 by 1 mM L-cysteine, 1 mM N-acetyl-L-cysteine, or 0.5 mM oxidized glutathione was significant, while other compounds showed no inhibition.

3.7. Effect of L-serine on the sensitivity of EhSATs to L-cysteine inhibition

We also directly tested whether the three SAT enzymes are differentially inhibited by L-cysteine in the presence of the physiological L-serine concentrations. L-Cysteine at the concentrations of 5–500 μM remarkably inhibited EhSATs in the presence of 0.5 mM of L-serine (Fig. 4 and Table 1). In contrast, in the presence of 3 mM of L-serine, which was equivalent to the concentration in the axenically cultured trophozoites (3.2 mM), [35], L-cysteine at the same concentrations showed much less inhibition (Fig. 5). Thus, not only the L-cysteine, but also L-serine (and acetyl-CoA, data not shown) concentration affects the EhSAT activity. At known L-cysteine and L-serine concentrations in axenically cultured trophozoites (0.3 and 3.2 mM, respectively), EhSAT1 and EhSAT2 activity was inhibited by approximately 90 or 20%, respectively, while EhSAT3 activity remained fully active. These data suggest that the activity of EhSAT1 and EhSAT2 is modulated under the *in vivo* conditions, where the L-serine and L-cysteine concentrations likely fluctuate.

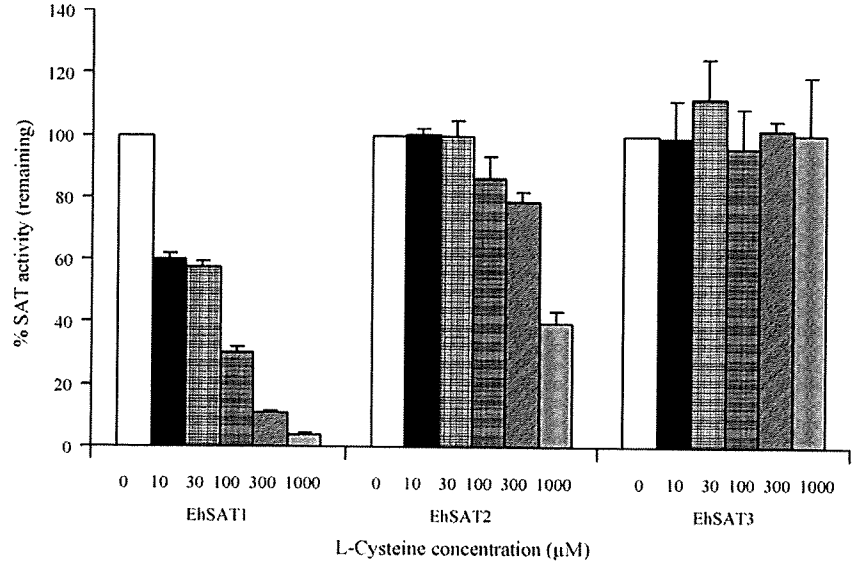

Fig. 5. Effects of various L-cysteine concentrations on the activity of EhSAT isotypes in the presence of physiological concentrations of L-serine (3 mM). The SAT activity is shown in percentage relative to that of the individual SAT isotype measured in the absence of L-cysteine.

3.8. Cellular distribution of EhSATs in E. histolytica trophozoites

We examined cellular distribution of three isotypes of EhSAT in the HM1 reference strain. The immunofluorescence imaging using antiserum raised against the corresponding recombinant protein showed that all the three isotypes are distributed to the cytosol (data not shown). We also verified the expression of EhSATs by immunoblots. The lysate was produced by freezing and thawing followed by sonication and centrifugation at 100,000 × *g* centrifugation (at 4 °C for 1 h). Immunoblots showed that EhSAT1 and 2 were fractionated to the soluble fraction (for clarity of immunoblots, the immunolots using a fraction which was obtained by further separation on anionic exchange chromatography is shown in Fig. 3C).

4. Discussion

In the present study, we have reported for the first time that *E. histolytica* possesses multiple isotypes of SAT with distinct properties. Although the presence of sulfur assimilatory cysteine biosynthetic pathway has been well documented in this parasite [18,36], and the feedback-inhibition of EhSAT1 by L-cysteine was previously reported [17], the existence of apparently redundant systems, consisting of multiple isoenzymes catalyzing identical reactions (i.e., EhSAT1-3 as well as CS isotypes, EhCS1-3, unpublished [18,20,37]), strengthen biological significance of regulation of L-cysteine synthesis in this organism. Although their subcellular localization has not been demonstrated, the lack of the organelle targeting signals, as seen in organelle-located SAT from plants [26,27], in EhSAT1-3 and the lack of the typical mitochondria and plastids in this organism [17] support the premise that the all three amoebic SAT isotypes are cytosolic. Immunofluorescence and cellular fractionation studies also suggest that all the three SAT isotypes are located to the cytosol. Isoform-dependent feedback-inhibition of SAT, often compartmentalized to the cytosol, chloroplast, and mitochondria, by L-cysteine was previously demonstrated in plants [8]. Thus, the present work is the first report showing the presence of multiple cytosolic SAT isoforms with distinct features.

The three SAT isotypes from *E. histolytica* showed high, intermediate, and low sensitivity to inhibition by L-cysteine. The sensitivity of EhSATs to the cysteine inhibition varies in two orders of magnitude (the K_i value of EhSAT1-3 was 4.7, 28, and 460 μM, respectively, Table 2). We have also shown that L-serine at the physiological concentrations modulates the sensitivity of EhSATs to L-cysteine. Furthermore, the modulation of the L-cysteine sensitivity by L-serine is isotype specific. Under the reported intracellular cysteine concentrations of axenically cultured trophozoites (0.3 mM), [35], the activity of EhSAT1 is predicted to be totally suppressed in this parasite. Alternatively, EhSAT1 may be compartmentalized to a confined region of the cytosol where the L-cysteine concentration is low. Although the intracellular L-serine and L-cysteine concentrations in the amoeba in the human remain unknown, it is conceivable that they vary under different conditions of its life cycle and infection, e.g., in the human colonic lumen and invaded tissues. Thus, the redundancy of CS/SAT and cysteine biosynthesis may be necessary to ensure replenishment of L-cysteine under various physiological and pathological conditions where the amino acid availability fluctuates.

In bacteria, L-cysteine at micromolar concentrations inhibits SAT activity and OAS acts not only as a substrate but also as an inducer of Cys regulon [5]. Since EhSAT3 is virtually insensitive to L-cysteine inhibition, L-cysteine production is not regulated unless EhSAT3 activity is regulated by other unidentified mechanisms including compartmentalization. Although roles of OAS remain totally promiscuous in this organism, it is plausible if OAS also regulates expression of genes involved in L-cysteine biosynthesis. It has been known in bacteria [5] under the L-cysteine-limited conditions, SATs do not only provide OAS for the replenishment of L-cysteine through desensitization of L-cysteine inhibition, but also induces the expression of genes involved in L-cysteine biosynthesis [38].

The previous transcriptome analysis [37] suggested all three EhSAT genes are expressed in axenic cultures; EhSAT1 and EhSAT3 are well expressed, while EhSAT2 is 10–40-fold less expressed than the other two isoforms. It was also demonstrated that expression of *EhSAT1* or *EhSAT2* gene was 3.4–6.0-fold downregulated or 4.1–8.7-fold upregulated, respectively, during the intestinal infection, whereas the expression of *EhSAT3* gene remained unchanged (only 1.5–1.6-fold repression). These data suggest that individual *EhSAT* genes are under coordinated regulation of expression under different physiological conditions and also that EhSAT2 might have a specific role in intestinal colonization.

Structural understanding of the in-sensitivity of EhSAT3 to the L-cysteine inhibition is underway. The carboxyl-terminal extension unique to EhSAT3 is one of the obvious points of interest involved in protein–protein interactions. The carboxyl-terminal region has also been implicated in the CS complex formation, as the 10–25 a.a. carboxyl-terminal truncation caused dissociation of SAT from CS in *E. coli* [39,40]. Further investigation of truncation and mutation by site-directed and PCR-based random mutagenesis, as shown in bacterial and plant SATs [39,41], is necessary. Finally, since the sulfur assimilatory cysteine biosynthetic pathway is absent from human, it should provide a suitable target for the rational development of new chemotherapeutics against amoebiasis. Recent demonstration of inhibition of *E. histolytica* trophozoites proliferation by compounds devised *in silico* by docking to *E. coli* SAT (NCI 128884, 29607, and 653543) [42] reinforced the premise. Therefore, the detailed study of its components, as shown in the present study, is important to validate the suitability of the target.

Acknowledgements

We thank Dan Sato, Afzal Husain, and all other members of our laboratory for the technical assistance and valuable discussions. This work was supported by a fellowship from the Japan Society for the Promotion of Science to S.H. (P06240), Grant-in-Aids for Scientific Research from the Ministry of Education, Culture, Sports, Science and Technology of Japan to V.A. (19790303) and T.N. (18GS0314, 18050006, 18073001), a grant for research on emerging and re-emerging infectious diseases from the Ministry of Health, Labour and Welfare of Japan to T.N., and a grant for research to promote the development of anti-AIDS pharmaceuticals from the Japan Health Sciences Foundation to T.N.

References

[1] Saito K. Biosynthesis of cysteine. In: Singh B, editor. Plant amino acids: biochemistry and biotechnology. New York: Marcel Dekker; 1998. p. 267–91.
[2] Leustek T. Molecular genetics of sulfate assimilation in plants. Physiol Plant 1996;97:411–9.
[3] Hell R. Molecular physiology of plant sulfur metabolism. Planta 1997;202:138–48.
[4] Brunold C, Rennenberg H. Regulation of sulfur metabolism in plants: first molecular approaches. Prog Bot 1997;58:164–86.
[5] Kredich NM, Tomkins GM. The enzymic synthesis of L-cysteine in *Escherichia coli* and *Salmonella typhimurium*. J Biol Chem 1966;241:4955–65.
[6] Hesse H, Nikiforova V, Gakière B, Hoefgen R. Molecular analysis and control of cysteine biosynthesis: integration of nitrogen and sulphur metabolism. J Exp Bot 2004;55:1283–92.
[7] Saito K, Yokoyama H, Noji M, Murakoshi I. Molecular cloning and characterization of a plant serine acetyltransferase playing a regulatory role in cysteine biosynthesis from watermelon. J Biol Chem 1995;270:16321–6.
[8] Noji M, Inoue K, Kimura N, Gouda A, Saito K. Isoform-dependent differences in feedback regulation and subcellular localization of serine acetyltrans-

ferase involved in cysteine biosynthesis from *Arabidopsis thaliana*. J Biol Chem 1998;273:32739–45.
[9] Howarth JR, Roberts MA, Wray JL. Cysteine biosynthesis in higher plants: a new member of the *Arabidopsis thaliana* serine acetyltransferase small gene-family obtained by functional complementation of an *Escherichia coli* cysteine auxotroph. Biochem Biophys Acta 1997;1350:123–7.
[10] Murillo M, Foglia R, Diller A, Lee S, Leustek T. Serine acetyltransferase from *Arabidopsis thaliana* can functionally complement the cysteine requirement of a *cysE* mutant strain of *Escherichia coli*. Cell Mol Biol Res 1995;41: 425–33.
[11] Ruffet ML, Lebron M, Droux M, Douce R. Subcellular distribution of serine acetyltransferase from *Pisum sativum* and characterization of an *Arabidopsis thaliana* putative cytosolic isoform. Eur J Biochem 1995;227:500–9.
[12] Bogdanova N, Bork C, Hell R. Cysteine biosynthesis in plants: isolation and functional identification of a cDNA encoding a serine acetyltransferase from *Arabidopsis thaliana*. FEBS Lett 1995;358:43–7.
[13] Hell R, Bogdanova N. Characterization of a full-length cDNA encoding serine acetyltransferase from *Arabidopsis thaliana*. Plant Physiol 1995;109:1498.
[14] Roberts MA, Wray JL. Cloning and characterization of an *Arabidopsis thaliana* cDNA clone encoding an organellar isoform of serine acetyltransferase. Plant Mol Biol 1996;30:1041–9.
[15] World Health Organization/Pan American Health Organization. Report of a consultation of experts on amoebiasis. Weekly Epidemiol Rep 1997;72: 97–9.
[16] Nozaki T, Asai T, Kobayashi S, et al. Molecular cloning and characterization of the genes encoding two isoforms of cysteine synthase in the enteric protozoan parasite, *Entamoeba histolytica*. Mol Biochem Parasitol 1998;97:33–44.
[17] Nozaki T, Asai T, Sanchez LB, Kobayashi S, Nakazawa M, Takeuchi T. Characterization of the gene encoding serine acetyltransferase, a regulated enzyme of cysteine biosynthesis from the protist parasites *Entamoeba histolytica* and *Entamoeba dispar*. Regulation and possible function of the cysteine biosynthetic pathway in *Entamoeba*. J Biol Chem 1999;274:32445–52.
[18] Nozaki T, Ali V, Tokoro M. Sulfur-containing amino acid metabolism in parasitic protozoa. Adv Parasitol 2005;60:1–99.
[19] Loftus B, Anderson I, Davies R, et al. The genome of the protist parasite *Entamoeba histolytica*. Nature 2005;433:865–8.
[20] Clark CG, Alsmark UC, Tazreiter M, et al. Structure and content of the *Entamoeba histolytica* genome. Adv Parasitol 2007;65:51–190.
[21] Nozaki T, Tokoro M, Imada M, et al. Cloning and biochemical characterization of genes encoding two isozymes of cysteine synthase from *Entamoeba dispar*. Mol Biochem Parasitol 2000;107:129–33.
[22] Diamond LS, Harlow DR, Cunnick CC. A new medium for the axenic cultivation of *Entamoeba histolytica* and other *Entamoeba*. Trans R Soc Trop Med Hyg 1978;72:431–2.
[23] Clark CG, Diamond LS. Methods for cultivation of luminal parasitic protists of clinical importance. Clin Microbiol Rev 2002;15:329–41.
[24] Sambrook J, Russell DW. Molecular cloning: a laboratory manual. 2nd ed. Cold Spring Harbor: Cold Spring Harbor Laboratory Press; 2001.
[25] Bradford MM. A rapid and sensitive method for the quantitation of microgram quantities of protein utilizing the principle of protein–dye binding. Anal Biochem 1976;72:248–54.
[26] Baecker PA, Wedding RT. Purification of serine acetyltransferase, a component of a multienzyme complex, by immunoadsorption and selective dissociation of the complex. Anal Biochem 1980;102:16–21.
[27] Nakamura K, Hayama A, Masada M, Fukushima K, Tamura G. Purification and some properties of plant serine acetyltransferase. Plant Cell Physiol 1988;29:689–93.
[28] Saito K, Miura N, Yamazaki M, Hirano H, Murakoshi I. Molecular cloning and bacterial expression of cDNA encoding a plant cysteine synthase. Proc Natl Acad Sci USA 1992;89:8078–82.
[29] Thompson JD, Higgins DG, Gibson TJ. CLUSTAL W: improving the sensitivity of progressive multiple sequence alignment through sequence weighting, position-specific gap penalties and weight matrix choice. Nucleic Acids Res 1999;22:4673–80.
[30] Kumar S, Tamura K, Jakobsen IB, Nei M. MEGA2: molecular evolutionary genetics analysis software. Bioinformatics 2001;17:1244–5.
[31] Pye VE, Tingey AP, Robson RL, Moody PC. The structure and mechanism of serine acetyltransferase from *Escherichia coli*. J Biol Chem 2004;279:40729–36.
[32] Olsen LR, Huang B, Vetting MW, Roderick SL. Structure of serine acetyltransferase in complexes with CoA and its cysteine feedback inhibitor. Biochemistry 2004;43:6013–9.
[33] Francois JA, Kumaran S, Jez JM. Structural basis for interaction of *O*-acetylserine sulfhydrylase and serine acetyltransferase in the *Arabidopsis* cysteine synthase complex. Plant Cell 2006;18:3647–55.
[34] Anderson I, Loftus B. *Entamoeba histolytica*: observations on metabolism based on the genome. Exp Parasitol 2005;110:173–7.
[35] Bakker-Grunwald T, Martin JB, Klein G. Characterizing of glycogen and amino acid pool of *Entamoeba histolytica* by 13C-NMR spectroscopy. J Euk Microbiol 1995;42:346–9.
[36] Ali V, Nozaki T. Current therapeutics, their problems, and sulfur-containing amino acid metabolism as a novel target against infections by "amitochondriate" protozoan parasites. Clin Microbiol Rev 2007;20:164–87.
[37] Gilchrist CA, Houpt E, Trapaidze N, et al. Impact of intestinal colonization and invasion on the *Entamoeba histolytica* transcriptome. Mol Biochem Parasitol 2006;147:163–76.
[38] Kredich NM. *Escherichia coli* and *Salmonella*. In: Curtiss R, Ingraham JL, Lin ECC, Low KB, Magasanik B, Reznikoff WS, Riley M, Schaechter M, Umbarger HE, editors. Cellular and molecular biology. American Society for Microbiology Press; 1996. p. 514–27.
[39] Mino K, Yamanoue T, Sakiyama T, Eisaki N, Matsuyama A, Nakanishi K. Purification and characterization of serine acetyltransferase from *Escherichia coli* partially truncated at the C-terminal region. Biosci Biotechnol Biochem 1999;63:168–79.
[40] Mino K, Yamanoue T, Sakiyama T, Eisaki N, Matsuyama A, Nakanishi K. Effects of bienzyme complex formation of cysteine synthetase from *Escherichia coli* on some properties and kinetics. Biosci Biotechnol Biochem 2000;64:1628–40.
[41] Denk D, Bock A. L-Cysteine biosynthesis in *Escherichia coli*: nucleotide sequence and expression of the serine acetyltransferase (cysE) gene from the wild-type and a cysteine-excreting mutant. J Gen Microbiol 1987;133:515–25.
[42] Agarwal SM, Jain R, Bhattacharya A, Azam A. Inhibitors of *Escherichia coli* serine acetyltransferase block proliferation of *Entamoeba histolytica* trophozoites. Int J Parasitol 2008;38:137–41.

Cellular Microbiology (2009) 11(10), 1471–1491

doi:10.1111/j.1462-5822.2009.01341.x
First published online 29 June 2009

Phosphatidylinositol-phosphates mediate cytoskeletal reorganization during phagocytosis via a unique modular protein consisting of RhoGEF/DH and FYVE domains in the parasitic protozoon Entamoeba histolytica

Kumiko Nakada-Tsukui, Hiroyuki Okada, Biswa Nath Mitra and Tomoyoshi Nozaki*
Department of Parasitology, National Institute of Infectious Diseases, 1-23-1 Toyama, Shinjuku-ku, Tokyo 162-8640, Japan.

Summary

To understand the roles of phosphoinositides [PtdIns] in phagocytosis of parasitic eukaryotes, we examined the interaction of phosphatidylinositol-3-phosphate [PtdIns(3)P] and putative PtdIns-P-binding proteins during phagocytosis in the enteric protozoan parasite Entamoeba histolytica. It was previously shown that phagocytosis in E. histolytica is indispensable for virulence and is inhibited by PtdIns 3-kinase inhibitors. We demonstrated by time-lapse live imaging that during the initiation of phagocytosis, the PtdIns(3)P biomarker GFP–Hrs–FYVE, was translocated to the phagocytic cup, phagosome, and to tunnel-like structures connecting the plasma membrane and phagosomes. E. histolytica possesses 12 FYVE domain-containing proteins (EhFP1-12), 11 of which also contain the RhoGEF/DH domain. Among them EhFP4 was shown to be recruited to the tunnel-like structures and to the proximal region of the phagosome. We further demonstrated that EhFP4 physically interacted with 4 of 10 predominant Rho/Rac small GTPases. Phosphoinositide binding assay showed that EhFP4 unexpectedly bound to PtdIns(4)P via the carboxyl-terminal domain and that the FYVE domain modulates the binding specificity of EhFP4 to PtdIns-P. Expression of the FYVE domain from EhFP4 inhibited phagocytosis while enhancement was observed when mammalian Hrs–FYVE domain was expressed. Altogether, we demonstrated that PtdIns(3)P, PtdIns(4)P and EhFP4 coordinately regulate phagocytosis and phagosome maturation in this parasitic eukaryote.

Received 10 March, 2009; revised 19 May, 2009; accepted 1 June, 2009. *For correspondence. E-mail: nozaki@nih.go.jp; Tel. (+81) 3 5285 1111 ext. 2600; Fax (+81) 3 5285 1219 or 1173.

Introduction

Entamoeba histolytica is a major cause of colitis and liver abscess in developing countries (Haque *et al.*, 2003; Ackers and Mirelman, 2006). Recently, several molecules playing fundamental roles in the biology and virulence of this parasite have been identified. Among them are the cell surface galactose/*N*-acetylgalactosamine-specific lectins, cysteine proteases and amoebapores, which are involved in the interaction with host cells and bacteria, the destruction of immune and non-immune cells, or in the digestion of ingested microorganisms respectively (Que and Reed, 2000; Frederick and Petri, 2005). In addition to these molecules, phagocytosis and motility have been shown to play a pivotal role in the establishment of infection (Labruyere and Guillen, 2006). It was demonstrated that phagocytosis and cell movement are controlled by the cytoskeleton and its regulators, including actins, myosins, p21 activated kinases and Rho/Rac small GTPases (Guillen *et al.*, 1998; Voigt and Guillen, 1999; Labruyere *et al.*, 2003; Coudrier *et al.*, 2005; Marion *et al.*, 2005; Arias-Romero *et al.*, 2006; Franco-Barraza *et al.*, 2006). Rho guanine nucleotide exchange factor (RhoGEF), the activator of Rho/Rac small GTPases, is also important in regulating biological processes where cytoskeletal reorganization is involved, including chemotaxis, cytokinesis, tumorigenesis and phagocytosis (Rossman *et al.*, 2005; Vargas and Gonzalez-de la Rosa, 2007). The number of RhoGEFs in the *E. histolytica* and human genomes are also comparable. Sixty-two RhoGEFs have been identified in *E. histolytica*, all belonging to the Dbl homology (DH) protein family, while 69 RhoGEFs are present in man (Vargas and Gonzalez-de la Rosa, 2007).

It should be emphasized that the molecular mechanisms of phagocytosis in *E. histolytica* are significantly divergent from well-established models found in other organisms, particularly to the professional phagocytes of mammals. First, among three main elements of the eukaryotic cytoskeleton, *E. histolytica* seems heavily dependent on actin microfilaments (Loftus *et al.*, 2005; Clark *et al.*, 2007). *E. histolytica* has a number of actin binding proteins to modify filamentous actins and highly conserved Arp2/3 complex, but lacks WASP/SCAR proteins, for actin nucleation by the Arp2/3 complex. Second, *E. histolytica* has only two myosins, myosin IB and myosin II, and lacks other myosins, like myosin V, that are considered ubiquitous (Labruyere and Guillen, 2006). Third, the involvement of Rab5 and Rab7A small GTPases in the formation of the prephagosomal vacuole during phagosome maturation is unique to *E. histolytica* (Saito-Nakano *et al.*, 2004; 2007; Nakada-Tsukui *et al.*, 2005). Fourth, phagosome acidification proceeds very rapidly and is completed within 2–5 min (Saito-Nakano *et al.*, 2004; Mitra *et al.*, 2005; 2006). These remarkable differences in the kinetics of phagosome maturation and the diversity of molecules involved in the process strongly suggest that the underlying mechanisms of phagocytosis and phagosomal maturation in this organism may be significantly divergent.

Recently, membrane phospholipids have been shown to play a pivotal role as mediators of membrane trafficking, cytoskeletal re-arrangement and cell surface receptor signalling (Lindmo and Stenmark, 2006). Membrane phosphatidylinositol (PtdIns) metabolism, in particular, has also been implicated in the regulation of phagocytosis (Fratti *et al.*, 2001; Botelho *et al.*, 2004; Scott *et al.*, 2005; Yeung *et al.*, 2006). In addition, phagosome maturation is blocked when phosphatidylinositol-3-phosphate [PtdIns(3)P] generation on the phagosome membrane is inhibited. Under normal conditions, the formation of PtdIns(3)P on the surface of phagosomes subsequently results in the recruitment of PtdIns(3)-P-binding proteins, including early endosome antigen-1 (EEA1) and hepatocyte growth factor-regulated tyrosine kinase substrate (Hrs) (Gillooly *et al.*, 2001; Chua and Deretic, 2004; Vieira *et al.*, 2004). Altogether, these studies indicate that PtdInss are important regulators of phagocytosis and phagosome maturation.

PtdIns(3)P was also implicated in the phagocytosis and endocytosis of *E. histolytica*, in a study where wortmannin, a potent inhibitor for phosphatidylinositol 3-kinase, was used (Ghosh and Samuelson, 1997; Powell *et al.*, 2006). However, *E. histolytica* lacks PtdIns(3)P effectors found in other organisms, including EEA1 and Hrs (Loftus *et al.*, 2005; Clark *et al.*, 2007). To better understand the involvement of lipid mediators in *E. histolytica*, and to uncover the molecular mechanism behind the inhibition of phagocyosis by wortmannin, we investigated the role of PtdIns(3)P and PtdIns-phosphate (PtdIns-P)-binding proteins during phagocytosis in *E. histolytica*. We have chosen to study PtdIns(3)P first because it has been implicated as the major regulator of endosome and phagosome maturation (Botelho *et al.*, 2004; Lindmo and Stenmark, 2006; Yeung *et al.*, 2006), and the specific biomarker for PtdIns(3)P is readily available (Gillooly *et al.*, 2000; Balla, 2005). A genome-wide survey of the *E. histolytica* database has shown that 12 FYVE (Fab-1, YGL023, Vps27, EEA1) domain-containing proteins are present in this organism, 11 of which reveal a unique modular structures consisting of the RhoGEF, pleckstrin homology (PH) and FYVE domains. We demonstrate the unique kinetics of PtdIns(3)P in phagocytosis by time-lapse live monitoring of PtdIns(3)P using a transgenic cell line expressing green fluorescent protein (GFP)-fused with the FYVE domain from Hrs. We subsequently demonstrate that among the 12 *E. histolytica* FYVE-domain-containing proteins (EhFP1-12), EhFP4 is specifically recruited to the phagocytic cup upon internalization of a mammalian cell, and is colocalized with F-actin. We further show that the unexpected phosphoinositide specificity of EhFP4 is mediated by its unique carboxyl terminal region, and that four Rho/Rac small GTPases serve as the downstream effectors of EhFP4.

Results

PtdIns(3)P is localized on the membrane of internal vesicles in the quiescent state, and not primarily in endosomes

We examined the kinetics of PtdIns(3)P, which is known to be involved in endosome and phagosome maturation in other organisms (Gillooly *et al.*, 2001), during endocytosis and phagocytosis in *E. histolytica*. To this end, we generated an *E. histolytica* transformant expressing GFP fused with the FYVE (Fab-1, YGL023, Vps27, EEA1) domain from hepatocyte growth factor 1-regulated tyrosine kinase substrate (Hrs), which has been used in other studies to probe the localization of PtdIns(3)P (Burd and Emr, 1998; Gaullier *et al.*, 1998; Gillooly *et al.*, 2000; Ellson *et al.*, 2001; Balla, 2005; Halet, 2005). The expression of the GFP–Hrs–FYVE fusion protein as a homogeneous 52 kDa protein was confirmed by immunoblot (Fig. 1A). Confocal photomicrographs revealed that the GFP–Hrs–FYVE signal was restricted to the membrane of a limited number of internal vesicles/vacuoles (Fig. 1B, a–c). It was shown that in mammalian cells, PtdIns(3)P is localized to the membrane of early endosomes and to the internal membranes of multivesicular endosomes, suggesting the general involvement of PtdIns(3)P in the endocytic pathway (Gillooly *et al.*, 2000).

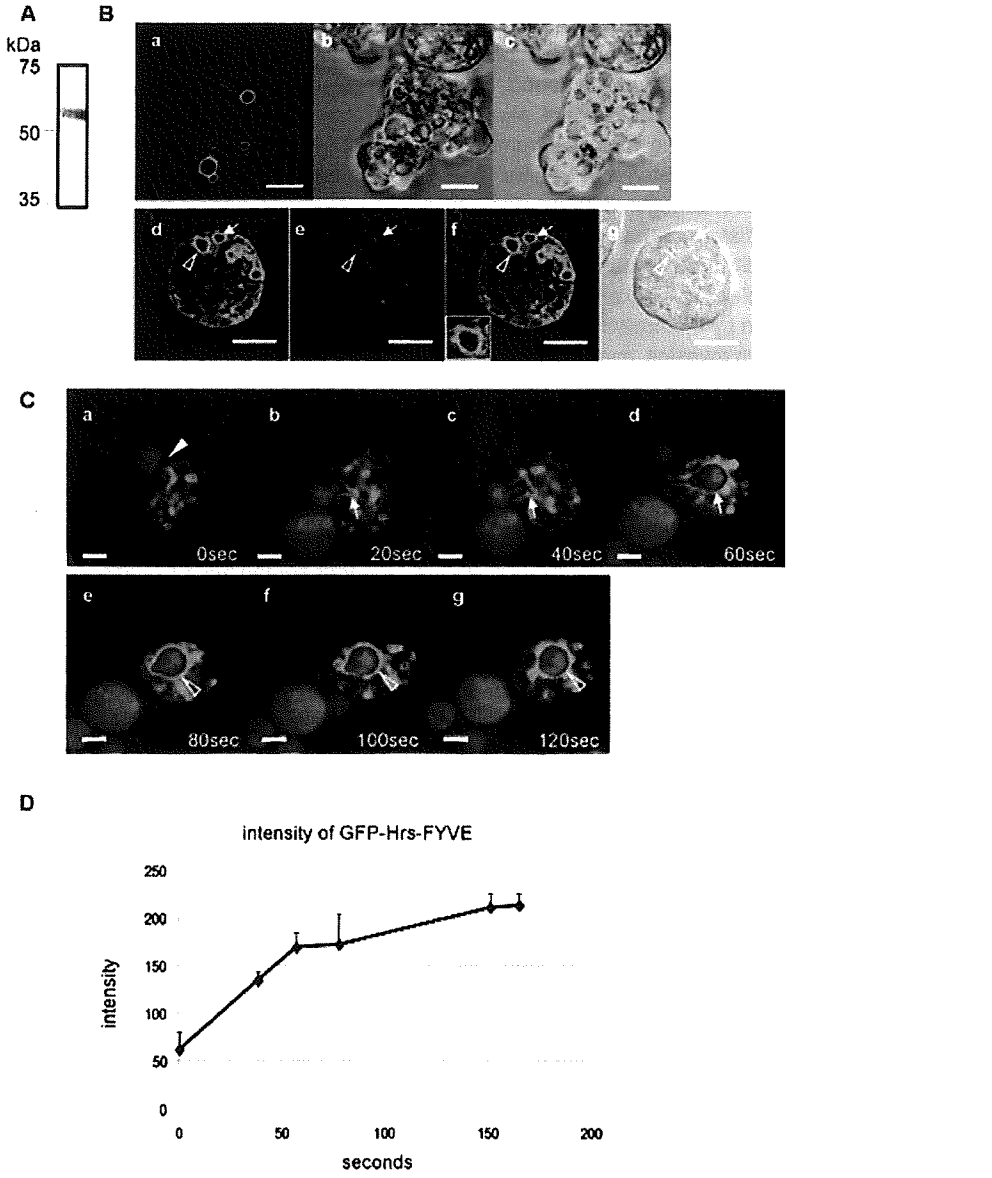

Fig. 1. Expression and localization of GFP–Hrs–FYVE in *E. histolytica*.
A. Immunoblot of the lysate from a *E. histolytica* transformant expressing GFP–Hrs–FYVE. A single 52 kDa band corresponding to myc-GFP–Hrs–FYVE fusion protein was detected by immunoblot analysis using anti-myc antibody.
B. Localization of GFP–Hrs–FYVE in the quiescent stage (a–c) and lack of colocalization of a fluid-phase marker, RITC-dextran (d–g). GFP–Hrs–FYVE-expressing *E. histolytica* trophozoites were fixed and analysed by Zeiss LSM 510. (a–c) GFP–Hrs–FYVE is localized on internal vesicles/vacuoles in the quiescent stage [a, GFP; b, differential interference contrast (DIC); c, merge]. (d–g) GFP–Hrs–FYVE expressing transformants were incubated with 2 mg ml ^{1} RITC-dextran for 10 min, fixed, and examined. (d, GFP; e, RITC-dextran; f, merge; g, DIC). Arrows indicate primary endosomes with PtdIns(3)P, open arrowheads indicate multivesicular bodies or secondary endosomes associated with PtdIns(3)P. A highly magnified image of a representative endosome-containing vacuole (open arrowheads) is shown in an islet (f). Bars, 10 m.
C. Time-lapse images of localization of GFP–Hrs–FYVE during CHO cell phagocytosis. CHO cells were labelled with Cell tracker blue and added to the GFP–Hrs–FYVE-expressing *E. histolytica* culture (approximately 1:2 ratio). Images were captured by Leica AS-MDW at given times. The exact timing of attachment of CHO cell by *E. histolytica* was manually monitored and defined as time 0. A filled arrowhead marks the attachment point between the *E. histolytica* and a CHO cell. Arrows depict the phagocytic cups and open arrowheads indicate phagosomes containing CHO cells. Bars, 10 m.
D. The kinetics of GFP–Hrs–FYVE recruitment on the nascent phagosome. The GFP fluorescence of the phagocytic cup and phagosome was measured using the *profile tool* in the Carl Zeiss LSM510. The mean and standard deviation of five random measurements are shown. Representative fluorescence profiles of a phagosome at two time points (0.2 and 164.4 s) are shown in Fig. S1.

To examine the association of PtdIns(3)P in the endocytic pathways in *E. histolytica*, the GFP–Hrs–FYVE-expressing transformant was incubated with 2 mg ml^{-1} RITC-dextran for 5, 10, 30, 60 and 90 min to allow endocytosis to take place. The number of RITC-dextran-containing endosomes associated or not associated with GFP–FYVE was counted, and the percentage of GFP–FYVE positive endosomes was calculated. At each time point, 14.0 ± 15.3%, 7.3 ± 7.9%, 1.4 ± 2.5%, 1.3 ± 0.8% and 2.0 ± 1.4% of the endosomes containing RITC-dextran were found to be associated with PtdIns(3)P respectively (Fig. 1B, d–g). The majority of the PtdIns(3)P-positive vacuoles contained RITC-dextran-positive vesicles in a confined area (Fig. 1B, f, islet), suggestive of multivesicular bodies (Saito-Nakano *et al.*, 2004). These data suggest that PtdIns(3)P is partially associated with endocytosis in the early phase and with multivesicular body formation. The majority of endosomes, however, are not associated with PtdIns(3)P during the steady state in this organism. The specificity of the Hrs–FYVE domain to PtdIns(3)P was verified by the phospholipid binding assay (see below, Fig. 4B, a).

Rapid recruitment of PtdIns(3)P to the phagocytic cup and phagosomes during phagocytosis of CHO cells

To investigate the involvement of PtdIns(3)P signalling in phagocytosis and phagosome maturation, we examined the localization of PtdIns(3)P during the course of engulfment of CHO cells. Cell tracker-loaded CHO cells were mixed with the amoeba transformants and the dynamics of PtdIns(3)P during their interaction and subsequent phagocytosis of CHO cells were monitored by real-time live imaging. We observed two types of phagocytosis based on their kinetics. Two-thirds (64.2 ± 6.8%) of the observed phagocytic events were completed within 3 min ('fast phagocytosis'), while one quarter (26.6 ± 7.3%) required more than 10 min to be completed ('slow phagocytosis') (K. Nakada-Tsukui, unpublished). In both types of phagocytosis, PtdIns(3)P was recruited to the phagocytic cup and phagosomes. The kinetics of PtdIns(3)P during the fast phagocytosis was as follows: less than 20 s after the adherence of the CHO cells, PtdIns(3)P started to accumulate on the phagocytic cup, and upon closure of the phagosome, PtdIns(3)P extended along the entire phagosome membrane (Fig. 1C and Video S1). The kinetics of the recruitment of GFP–Hrs–FYVE on the nascent phagosome was further analysed (Fig. 1D and Fig. S1). A time-dependent linear accumulation of the GFP signal was observed up to 160 s. In 'fast phagocytosis', the entire process from the formation of the phagocytic cup to the closure of the phagosome membrane was completed within 80 s. In this example, PtdIns(3)P remained on the phagosome membrane for at least 1 h after the closure of the phagosome.

In 'slow phagocytosis', instead of internalizing the CHO cell as a whole, *E. histolytica* gradually internalized its content through a narrow tunnel that was generated upon adherence (Video S2). This tunnel-like structure, containing a small portion of CHO cell, often persisted for more than 30 min without closure of the phagocytic cup. During this process, PtdIns(3)P also accumulated on the phagocytic cup right after the internalization, and remained on both the tunnel-like structure and the phagosome membrane. As shown in Videos S1 and S2, thread-like structures were often observed to be associated with GFP–Hrs–FYVE between PtdIns(3)P-positive vacuoles. These PtdIns(3)P-associated thread-like structures were seldom observed during the quiescent stage, suggesting that phagocytosis-induced PtdIns(3)P signalling is likely involved in the formation of these structures.

The 'slow phagocytosis' demonstrated here was also described in earlier studies in *Entamoeba* (Lejeune and Gicquaud, 1987; 1992), and appears to be similar to the PtdIns 3-kinase-dependent constriction of phagosomes described by Swanson *et al.* (1999). This observation may reflect the inability to complete the phagocytic process normally.

We further calculated the percentage of phagosomes associated with PtdIns(3)P during phagocytosis. GFP–Hrs–FYVE expressing amoebas were co-cultured with Cell tracker blue-loaded CHO cells for 10, 30 and 60 min. The phagosomes and phagocytic cups positive for GFP–Hrs–FYVE were counted under a confocal microscope. At 10, 30 and 60 min of cocultivation, 69 ± 6.7%, 51 ± 4.5% and 27 ± 5.7% of phagosomes were associated with PtdIns(3)P while 75% of the phagocytic cups were also PtdIns(3)P positive (Fig. S2). Although we did not distinguish fast and slow phagocytosis in this experiment, PtdIns(3)P association was predominantly observed on the phagosomes at the early time points of phagocytosis and also on the phagocytic cups. These results suggest that phagocytosis predominantly (> 70% of the phagocytosis events) occurs in a PtdIns(3)P-dependent manner.

Expression of GFP–Hrs–FYVE does not affect endocytosis, phagosome acidification and degradation of internalized materials in the phagosomes

To exclude the possibility that expression of GFP–Hrs–FYVE affects the normal kinetics of phagosome maturation, e.g. acidification and degradation of its content, we examined the kinetics of the phagosome pH in the red fluorescent protein (RFP)-Hrs–FYVE-expressing and control RFP-expressing transformants, by the previously described method using FITC-conjugated yeasts (Mitra *et al.*, 2005; 2006; Saito-Nakano *et al.*, 2007). The

kinetics of the phagosomal pH in these transformants was similar to each other (B.N. Mitra, data not shown), and also to that of the wild-type amoeba (Mitra *et al.*, 2005). We also compared the kinetics of degradation of an ingested *Leishmania* promastigote expressing GFP in a phagosome by measuring fluorescence intensity (Mitra *et al.*, 2005; 2006; Saito-Nakano *et al.*, 2007). Similar to the results of the acidification kinetics, the kinetics of GFP decay of ingested *Leishmania* parasites in both transformants was comparable (B.N. Mitra, data not shown). Thus, expression of the Hrs–FYVE domain does not affect phagosome maturation and degradation of endocytosed materials in the phagosomes.

We further examined if endocytosis is affected by GFP–Hrs–FYVE expression. The rate of endocytosis of RITC-dextran was indistinguishable between the GFP and GFP–Hrs–FYVE transformants (K. Nakada-Tsukui, data not shown). Thus, although we were not able to examine colocalization of RITC-dextran and GFP–Hrs–FYVE at the very early time points (less than 5 min) due to technical problems, we are tempted to conclude that PtdIns(3)P is not primarily involved in endocytosis.

Expression of 12 FYVE domain-containing proteins in E. histolytica

To get more insights into the downstream effectors of PtdIns(3)P during phagocytosis, we performed a genome-wide search for FYVE domain-containing proteins in the *E. histolytica* genome database (http://www.tigr.org/tdb/e2k1/eha1/). The FYVE domain derived from Hrs (Komada *et al.*, 1997) was used as a query sequence. Twelve *E. histolytica* proteins showed significant homology (*E*-value < 1.1 10 ^{3}), and we named these proteins EhFP1-12: *E. histolytica* FYVE domain-containing proteins 1–12. Eleven EhFP proteins (EhFP1-11) showed a similar overall structure, containing RhoGEF/DH and PH domains at the amino terminus of the FYVE domain (Fig. 2A). This modular structure containing RhoGEF/DH indicates that these FYVE domain proteins likely modulate cytoskeletal re-arrangement downstream of PtdIns(3)P signalling (Rossman *et al.*, 2005). An expanded repertoire of EhFP gene family suggests the importance of PtdIns-P-mediated signalling in this organism.

The levels of transcription of the EhFP genes were examined using DNA microarray. Total RNA from a reference HM-1:IMSS strain was prepared and hybridized to a custom-made *E. histolytica* DNA microarray (Gilchrist *et al.*, 2006; Ehrenkaufer *et al.*, 2007). Transcriptional levels of individual EhFP genes varied. EhFP5, 6, 7 and 10 were highly expressed (> 50% of the level of RNA polymerase II), while EhFP1, 2, 4, 8 and 12 were moderately expressed (between 20% and 50%), and EhFP3, 9 and 11 were poorly expressed (< 20%). EhFP9 protein was previously detected in phagosomes isolated from another clinical isolate (KU33 strain) by proteomic analysis (Okada *et al.*, 2006).

Intracellular localization of EhFPs and the dynamism of EhFP4 during phagocytosis

To understand the role of individual EhFPs in CHO cell phagocytosis, intracellular localization and their kinetics during phagocytosis were examined using transformants expressing HA-tagged EhFP proteins. Epitope-tag plasmid constructs, to express all EhFPs except EhFP9, and their corresponding transformants were successfully produced. We were unable to clone an EhFP9 protein coding region for unknown reasons despite repeated trials. Protein expression of HA-EhFP1, 2, 4 and 5 was confirmed by immunoblots, while expression of HA-EhFP3, 6, 7, 8, 10 and 12 failed (K. Nakada-Tsukui, unpublished). Analysis of EhFP11 was not included in this study because we found this entry in an updated TIGR database after completing all constructions. In the following experiments, we characterized EhFP1, 2, 4 and 5. The analysis of the remaining EhFPs will be described elsewhere.

Immunofluorescence imaging showed that HA-EhFP1, 2, 4 and 5 were localized throughout the cytoplasm in steady state (K. Nakada-Tsukui, unpublished). During CHO cell phagocytosis, localization of HA-EhFP1 and 2 did not change significantly (Fig. 2B). HA-EhFP5 was weakly associated with the phagocytic cup, and did not associate with the phagosome membrane at a later stage (Fig. 2B). On the other hand, HA-EhFP4 was recruited to the phagocytic cup and to a tunnel-like tubular structure, connecting the plasma membrane and the phagosome (Fig. 2C and Fig. S4). This tunnel-like structure was characteristically observed during 'slow phagocytosis.' The distribution of EhFP4 overlapped with that of F-actin, as demonstrated with anti-HA antibody and phallacidin double staining (Fig. 2D), suggesting the possible involvement of EhFP4 in actin re-arrangement.

Small GTPase RacG, p21 activated kinase PAK1, and calcium binding protein EhCaBP1 have been reported to be involved in phagocytosis (Guillen *et al.*, 1998; Labruyere *et al.*, 2003; Jain *et al.*, 2008). Among them, it was previously shown that upon erythrophagocytosis, EhCaBP1 was transiently recruited to the phagocytic cup and was dissociated from it less than one minute of engulfment (Jain *et al.*, 2008). We examined whether EhFP4 colocalizes with EhCaBP1 during CHO cell phagocytosis (Fig. 2E). Upon direct physical interaction with CHO cells, EhFP4 and EhCaBP1 both accumulated at the contact site (Fig. 2E, a–d). During internalization of CHO cells, the localization of EhCaBP1 appeared to be restricted to the proximal peripheral region of the

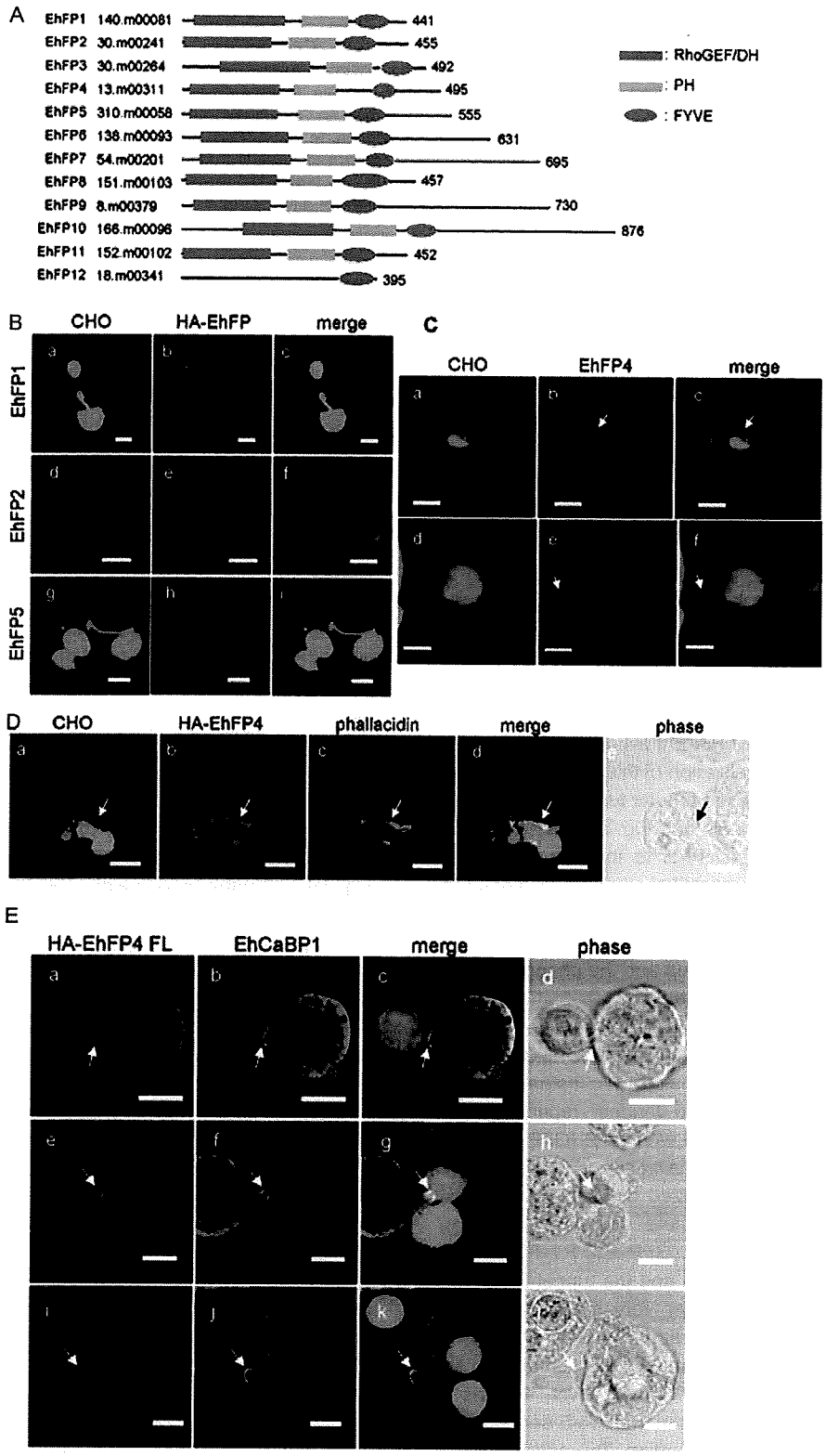
A
EhFP1 140.m00081 441
EhFP2 30.m00241 455
EhFP3 30.m00264 492
EhFP4 13.m00311 495
EhFP5 310.m00058 555
EhFP6 138.m00093 631
EhFP7 54.m00201 695
EhFP8 151.m00103 457
EhFP9 8.m00379 730
EhFP10 166.m00096 876
EhFP11 152.m00102 452
EhFP12 18.m00341 395
: RhoGEF/DH
: PH
: FYVE
B
CHO
HA-EhFP
merge
EhFP1
EhFP2
EhFP5
C
CHO
EhFP4
merge
D
CHO
HA-EhFP4
phallacidin
merge
phase
E
HA-EhFP4 FL
EhCaBP1
merge
phase

Fig. 2. FYVE domain-containing proteins in *E. histolytica* (EhFP) and localization of EhFP proteins during CHO cell phagocytosis.
A. A schematic representation of domain structures of EhFP proteins. RhoGEF/DH, pleckstrin homology, or FYVE domains are shown as red, green rectangles or blue ovals respectively. TIGR ID numbers and amino acid numbers of EhFP1–12 are shown.
B and C. Localization of EhFP1, 2, 4 and 5. Trophozoites of the HA-tagged EhFP1-, EhFP2-, EhFP5- (B) or EhFP4-expressing (C) transformants were co-cultured with Cell tracker green-loaded CHO cells for 30 min, fixed and reacted with anti-HA antibody, followed by Alexa-568 conjugated anti-mouse IgG secondary antibody. Bars, 10 m. Arrows (in C) indicate EhFP4 on the proximal portion of the phagosome (b, c, e and f) and the tunnel-like structures linked to the phagosome (e and f). Bars, 10 m.
D. Colocalization of EhFP4 and F-actin during CHO cell phagocytosis. HA-EhFP4-expressing trophozoites were co-cultured with Cell tracker blue-loaded CHO cells for 30 min, fixed and reacted with anti-HA and BODIPY FL phallacidin to visualize HA-EhFP4 and F-actin. Arrows indicate EhFP4 and F-actin accumulated at the proximal portion of the phagosome and the tunnel-like structures linked to the phagosome. Bars, 10 m.
E. Partial colocalization of EhFP4 and EhCaBP1 during CHO cell phagocytosis. HA-EhFP4-expressing *E. histolytica* were co-cultured with Cell tracker blue-loaded CHO cells for 30 min, fixed, and reacted with anti-HA antibody and anti-EhCaBP antibody. The cells were further reacted with Alexa-568 anti-mouse IgG and Alexa-488 anti-rabbit IgG secondary antibody. Arrows indicate regions where HA-EhFP4 and EhCaBP colocalize. Note that Cell tracker blue signal of CHO cells is also seen in the green channel. Bars, 10 m.

phagocytic cup, while EhFP4 was broadly distributed at the phagocytic cup and the tunnel-like structures (Fig. 2E, e–l).

Localization of EhFP4 to the phagocytic cup is mediated by the FYVE and the carboxyl-terminal (CT) domains

To examine whether the FYVE domain is involved in the EhFP4 recruitment during phagocytosis, a deletion mutant of HA-EhFP4 lacking the FYVE and CT domains, HA-EhFP4DH-PH, was generated. Expression of HA-EhFP4DH-PH protein was confirmed by Western blot analysis as a 40 kDa band and the level of its expression was comparable to that of HA-EhFP4 (K. Nakada-Tsukui, data not shown). The localization of this truncation mutant to the phagocytic cup and the tubular tunnel structure was remarkably reduced (Fig. 3A and Fig. S4). However, the recruitment of HA-EhFP4DH-PH to the phagocytic cup was not totally abolished most likely due to the interaction with other unidentified proteins that localize to the phagocytic cup. Taken together, these data suggest that EhFP4 is localized to the phagocytic cup and the phagosome via the FYVE domain and/or CT domain.

To perform live-imaging of EhFP4, we attempted to create an amoeba transformant expressing GFP full-length EhFP4 (EhFP4FL), but failed. We instead created a transformant expressing two tandem repeats of the FYVE domain of EhFP4 fused with GFP (GFP–EhFP4–FYVE), and examined its localization and dynamism. GFP–EhFP4–FYVE was localized diffusely to the cytoplasm under the quiescent state (Fig. 3B, a and b). During CHO cell phagocytosis, GFP–EhFP4–FYVE was recruited to the phagocytic cup and the tunnel-like structure (Fig. 3B, c–j), in a manner very similar to that of HA-EhFP4 (Figs 2C and 3A, and Fig. S4). This result supports the hypothesis that the FYVE domain mainly defines the localization of EhFP4. However, there is a possibility that domains other than the FYVE domain also have a role to define the localization. To understand the role of these domains of EhFP4 in localization and lipid binding, we next examined the lipid binding specificity.

Phosphoinositide specificity of EhFP4

To examine the specificity of EhFP4 towards various phosphoinositides and phospholipids. Lipid binding assay was performed using GST-fused Hrs-2xFYVE (GST–Hrs–FYVE), GST fusion proteins of EhFP4 FYVE, or CT domains (GST–EhFP4–FYVE or GST–EhFP4–CT respectively), and His tag-trigger factor (TF) fusion proteins of full-length EhFP4 (TF–EhFP4FL), FYVE/CT domain-deleted EhFP4 (TF–EhFP4DH–PH), and RhoGEF/DH domain of EhFP4 (TF–EhFP4DH) (Fig. 4B). As expected, GST–Hrs–FYVE showed specific binding to PtdIns(3)P and TF showed no interaction with phosphoinositides and phospholipids (Fig. 4B, a and b). Surprisingly, TF–EhFP4FL strongly bound to PtdIns(4)P, and weakly to PtdIns(3)P and PtdIns(5)P (Figs 4B, c). This interaction was not observed with TF-EhFP4 DH-PH, suggesting that the interaction occurs via the FYVE and/or CT domain(s) (Fig. 4B, d). Furthermore, neither TF–EhFP4DH nor GST–EhFP4–FYVE showed binding with phosphoinositides and phospholipids (Fig. 4B, e and f). This is in marked contrast with the specific binding of Hrs–FYVE to PtdIns(3)P (Gillooly *et al.*, 2000). The GST–EhFP4–CT protein unexpectedly bound to PtdIns(3)P, PtdIns(4)P and weakly to PtdIns(5)P (Fig. 4B, g). GST–EhFP4PH could not be produced in a soluble form (K. Nakada-Tsukui, unpubl. data).

To further confirm that the FYVE domain is not involved in the interaction of EhFP4 with phospholipids, we created TF-EhFP4 FL recombinant proteins in which one or two residues, shown to be involved in PtdIns(3)P binding or affect endosomal localization of EEA1, were mutated: His365Ser/His366Ser (HS) and Cys375Ser (CS) mutants (Stenmark *et al.*, 1996; 2002). Both the mutants equally bound to PtdIns(3)P, PtdIns(4) and PtdIns(5)P, in a similar fashion to TF–EhFP4FL (Fig. 4B, h and i).

EhFP4FLCS mutant was expressed as an amino-terminal HA fusion protein and its localization was examined by indirect immunofluorescence assay (Fig. 4C). The distribution of EhFP4FLCS mutant was indistinguishable from that of the wild-type. EhFP4FLCS mutant was distributed to the cytosol in steady state (Fig. 4C, a–d), and

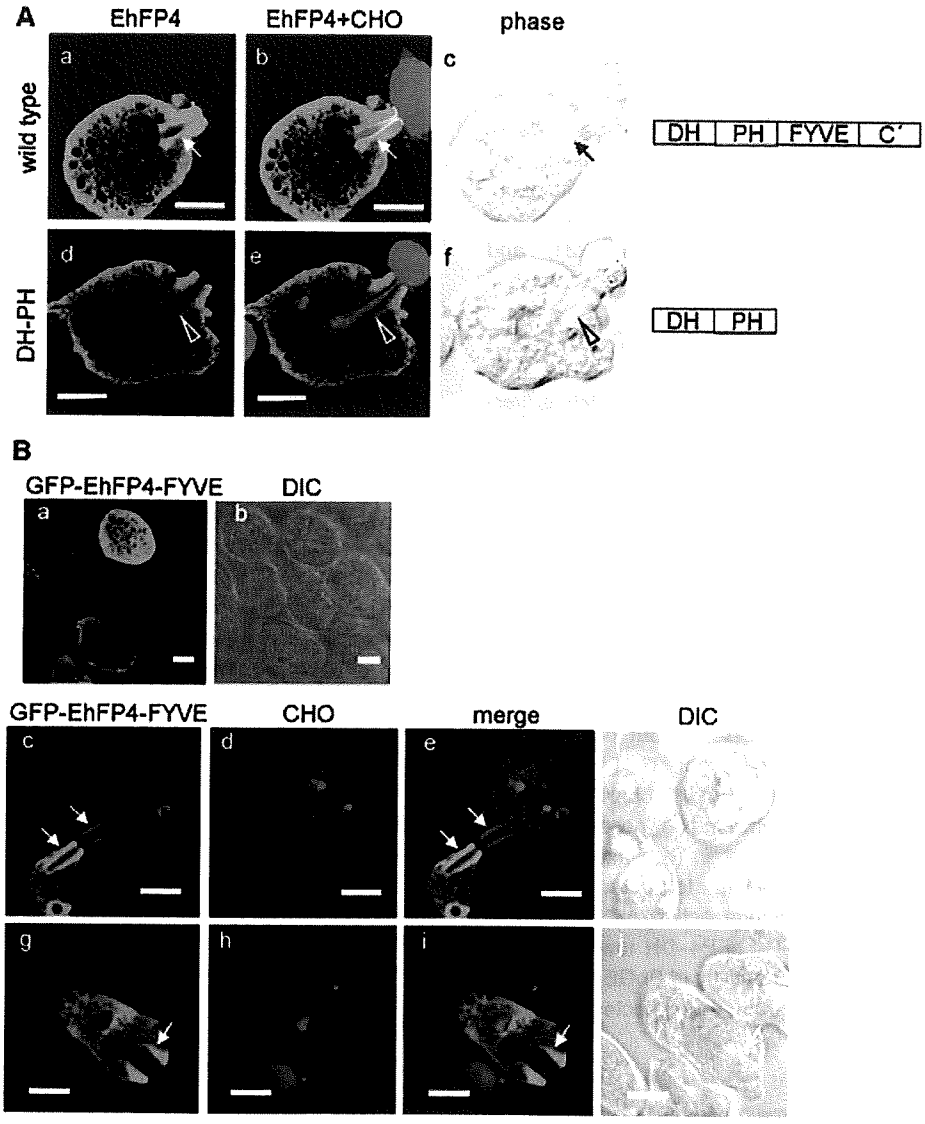

Fig. 3. Involvement of FYVE and CT domains in the EhFP4 recruitment to the phagocytic cup and the tunnel-like structure during phagocytosis.
A. Localization of wild-type EhFP4 (a–c) and mutant EhFP4 lacking FYVE domain ('DH-PH', d–f). Trophozoites of the transformants expressing HA-EhFP4 or HA-EhFP4DH-PH were co-cultured with Cell tracker orange-loaded CHO cells for 30 min, fixed, reacted with anti-HA antibody and Alexa-488 conjugated anti-mouse IgG secondary antibody. Arrows indicate HA-EhFP4 on the tunnel-like structure. Open arrowheads indicate the structures not associated with HA-EhFP4DH-PH. Bars, 10 m. Three additional trophozoites of wild-type EhFP4 and EhFP4DH-PH are also shown in Fig. S4.
B. Localization of GFP–EhFP4–FYVE in the quiescent state (before phagocytosis, a and b) and during phagocytosis (c–j). Arrows indicate GFP–EhFP4–FYVE on the tunnel-like structure. Bars, 10 m.

concentrated to the phagocytic cup and the tunnel-like structure (i–p), similar to the wild-type EhFP4 (Fig. 3B), while EhFP4FLCS mutant was not accumulated on phagosomes (Fig. 4C, e–h). Together, these data suggest that the EhFP4 recruitment to the phagocytic cup is mainly regulated by the phospholipid binding via the CT domain, and that the FYVE domain only modulates the specificity of the phospholipid binding of the EhFP4 CT domain.

Identification of Rho/Rac small GTPases as downstream effectors of EhFP4

The close association of EhFP4 with F-actin during phagocytosis, as shown in Fig. 2D, and the presence of the RhoGEF/DH domain in EhFP4 led us to speculate that EhFP4 mediates actin re-arrangement via activation of Rho/Rac small GTPases. Thus, we attempted to identify Rho/Rac proteins that interact with EhFP4. In the

E. histolytica genome database, 24 Rho/Rac genes were identified. Among them 10 highly transcribed Rho/Rac genes were selected based on a transcriptome analysis (Fig. 5A): 108.m00133 (EhRacC; Lohia and Samuelson, 1993), 52.m00167 (EhRho1; Lohia and Samuelson, 1996), 140.m00084, 146.m00106 (EhRacG; Guillen *et al.*, 1998), 16.m00303 (EhRacD; Lohia and Samuelson, 1993), 197.m00080 (EhRacA; Lohia and Samuelson, 1993), 296.m00051, 87.m00159, 46.m00231 and 69.m00185. Detailed analysis of the microarray study will be discussed elsewhere.

We examined physical interaction of TF–EhFP4FL, TF–EhFP4DH–PH or TF with GST-fused Rho/Rac proteins. It was previously shown that RhoGEF/DHs preferentially interact with the nucleotide-free form of Rho/Rac (Rossman *et al.*, 2005). Purified GST-Rho/Rac protein was immobilized with glutathione-Sepharose resin and bound guanine nucleotides were removed by EDTA treatment. The resin was then mixed with TF–EhFP4FL, TF–EhFP4DH–PH or TF. After washing, unbound and bound fractions were analysed by immunoblot analysis with anti-His or anti-GST antibodies (Fig. 5B). Four Rho/Rac molecules, 108.m00133 (EhRacC), 16.m00303 (EhRacD), 87.m00159 and 46.m00231, bound to both TF–EhFP4FL and TF–EhFP4DH–PH, but not with TF. Neither control GST–EhRab7A nor GST bound to TF–EhFP4FL, TF–EhFP4DH–PH or TF. 69.m00185 also showed weak, and inconsistent binding, possibly due to instability of the recombinant protein (K. Nakada-Tsukui, unpublished). We were unable to detect guanine nucleotide (GDP/GTP) exchange activity of TF-EhFP4, TF–EhFP4DH–PH or the TF–EhFP4–DH towards these Rho/Rac proteins, while GEF activity of EhGEF1 towards RacG (Aguilar-Rojas *et al.*, 2005), was detected under the same conditions.

Expression of the FYVE domain of EhFP4 represses phagocytosis of CHO cells and carboxylated beads

To get more insight into the role of FYVE domain of EhFP4 on CHO cell phagocytosis, we further examined whether expression of the FYVE domain of amoebic EhFP4 or mammalian Hrs affects phagocytosis. GFP–EhFP4–FYVE, GFP–Hrs–FYVE and GFP transformants were incubated with CHO cells or carboxylated beads to allow ingestion for 10, 30 and 60 min, and phagocytosis was analysed by flow cytometry. The percentage of amoebae that ingested CHO cells was remarkably affected by expression of GFP–EhFP4–FYVE or GFP–Hrs–FYVE at all time points (Fig. 6, top left). CHO cell phagocytosis was enhanced by 1.8- to 2.7-fold in the GFP–Hrs–FYVE transformant, and repressed by 50–60% in the GFP–EhFP4–FYVE transformant, when compared with the GFP transformant. In contrast, bead phagocytosis was 5–40% reduced by expression of either GFP–Hrs–FYVE or GFP–EhFP4–FYVE (Fig. 6, bottom).

Discussion

Role of PtdIns(3)P in membrane trafficking in E. histolytica

In this study, we demonstrated the localization of PtdIns(3)P in the pathogenic protist *E. histolytica*. During the quiescent state, PtdIns(3)P localizes to internal vesicles/vacuoles, but not primarily in early endosomes (Fig. 1). The minor contribution of PtdIns(3)P to endosome biosynthesis in this protist, which was also previously shown (Powell *et al.*, 2006), is in sharp contrast to mammals and yeasts, where PtdIns(3)P localizes to endosomes and multivesicular endosomes (Gillooly *et al.*, 2000). It has been well established that PtdIns(3)P functions as a mediator for the endosome and phagosome maturation by recruiting PtdIns(3)P binding proteins, i.e. EEA1 and Hrs, in mammals (Gillooly *et al.*, 2001; Chua and Deretic, 2004; Vieira *et al.*, 2004). Based on the available genome information, *E. histolytica* does not have these effectors, which may explain the lack of PtdIns(3)P association with endosomes. However, we cannot exclude the possibility that PtdIns(3)P is localized to the early endosomes only in the very early phase of endocytosis (within 5 min after internalization), and thus play an important, but transient role in endocytosis.

Powell and colleagues previously reported that during erythrophagocytosis PtdIns(3) accumulated on the phagocytic cup and peripheral phagosomes (i.e. phagosomes located close to the plasma membrane), but not on phagosomes located at the centre of the cell using GST 2xFYVE recombinant protein as a bioprobe (Powell *et al.*, 2006). We also observed that GFP–Hrs–FYVE localized to erythrocyte-containing phagosomes (Fig. S5). Since the same two tandem copies of the FYVE domain from human Hrs were used as a PtdIns(3)P biomarker in both the previous and present studies, the subtle discrepancy of the FYVE localization is most likely due to experimental differences for visualization of PtdIns(3)P. Fixed trophozoites were previously used to detect PtdIns(3)P reacted with GST 2xFYVE (Powell *et al.*, 2006), while we determined the location of PtdIns(3)P using live cells expressing GFP–Hrs–FYVE.

Possible mechanisms of PtdIns(3)P recruitment to the phagosome membrane

We demonstrated by time-lapse live imaging (Videos S1 and S2, and Fig. 1) that PtdIns(3)P was recruited to the newly formed phagosome right after ingestion and accumulated on the phagosome membrane. Ellson *et al.*

A

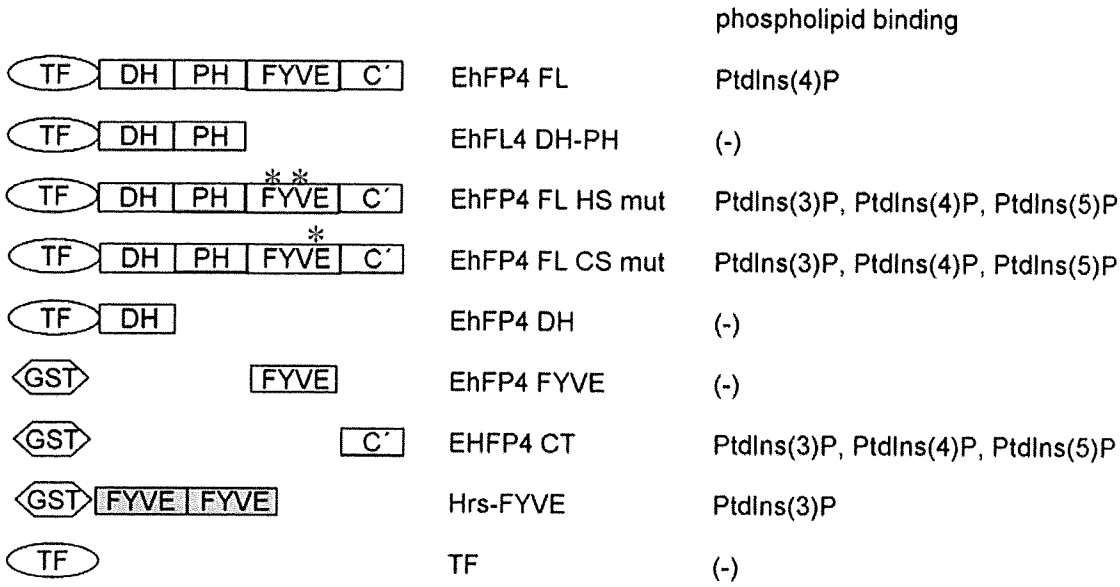
phospholipid binding
TF DH PH FYVE C´
EhFP4 FL
PtdIns(4)P
TF DH PH
EhFL4 DH-PH
(-)
TF DH PH FYVE C´
EhFP4 FL HS mut
PtdIns(3)P, PtdIns(4)P, PtdIns(5)P
TF DH PH FYVE C´
EhFP4 FL CS mut
PtdIns(3)P, PtdIns(4)P, PtdIns(5)P
TF DH
EhFP4 DH
(-)
GST FYVE
EhFP4 FYVE
(-)
GST C´
EHFP4 CT
PtdIns(3)P, PtdIns(4)P, PtdIns(5)P
GST FYVE FYVE
Hrs-FYVE
PtdIns(3)P
TF
TF
(-)

B

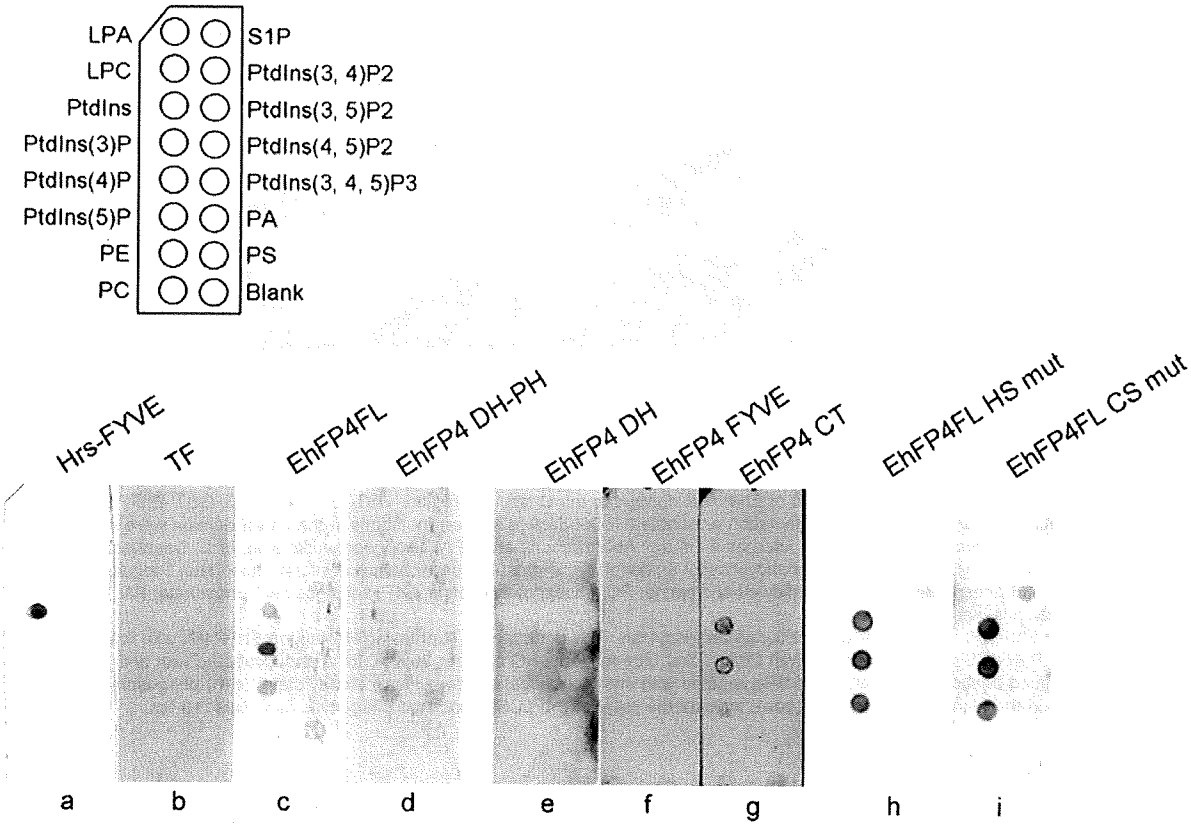
LPA
LPC
PtdIns
PtdIns(3)P
PtdIns(4)P
PtdIns(5)P
PE
PC
S1P
PtdIns(3, 4)P2
PtdIns(3, 5)P2
PtdIns(4, 5)P2
PtdIns(3, 4, 5)P3
PA
PS
Blank
Hrs-FYVE
TF
EhFP4FL
EhFP4 DH-PH
EhFP4 DH
EhFP4 FYVE
EhFP4 CT
EhFP4FL HS mut
EhFP4FL CS mut
a
b
c
d
e
f
g
h
i

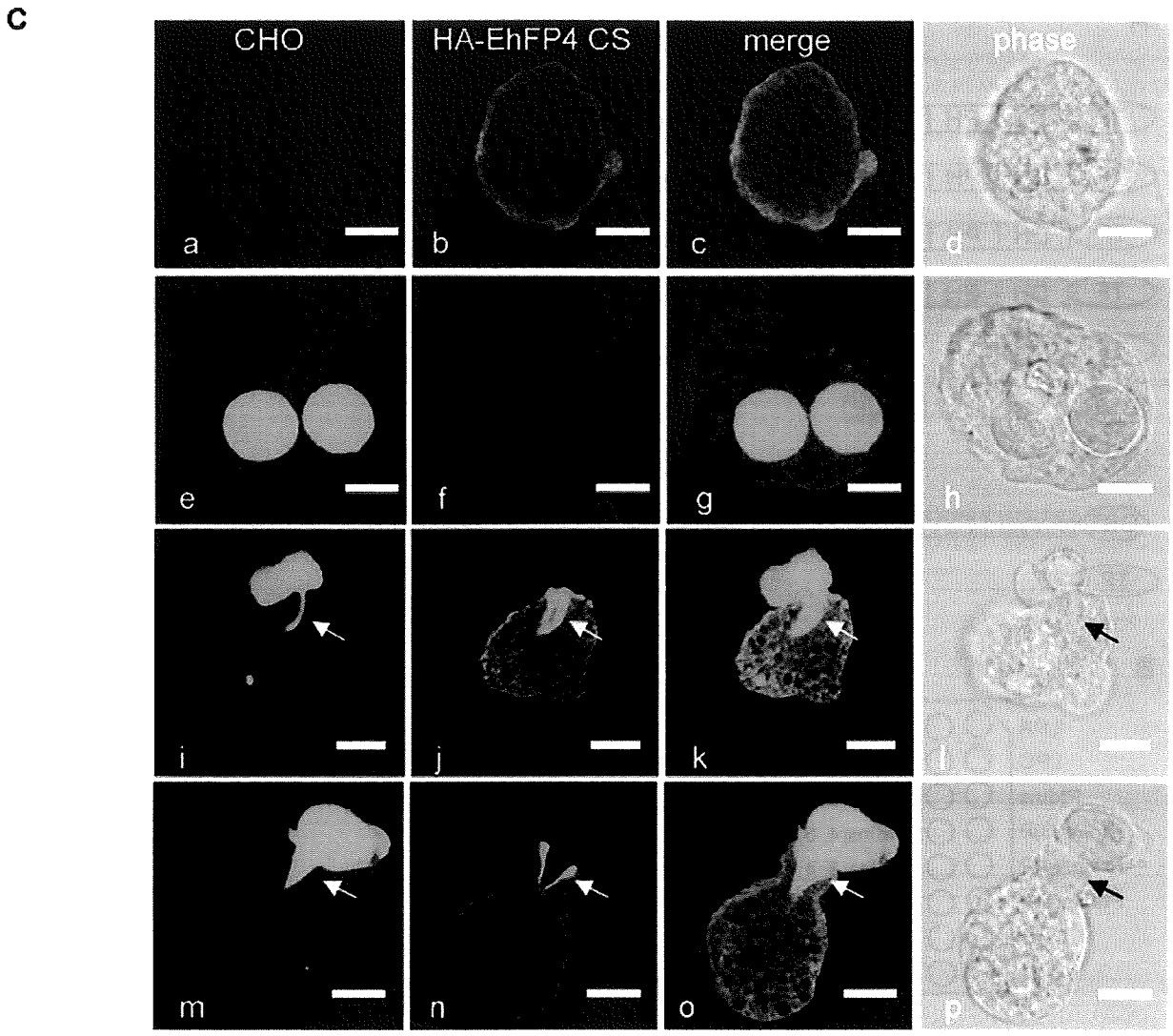

Fig. 4. Phospholipid specificity of EhFP4FL.
A. The domain structures and fusion partners of all the recombinant proteins used in the phospholipid binding study and their phospholipid specificities.
B. Phospholipid specificity of various recombinant proteins corresponding to the full-length or different domains of EhFP4. A GST fusion protein of Hrs–FYVE (GST–Hrs–FYVE) and a TF fusion protein of a full-length EhFP4 (TF–EhFP4FL), a TF fusion protein of EhFP4–DH domain (TF–EhFP4–DH), a GST fusion protein of Eh-FYVE domain or the C-terminal region (GST–EhFP4–FYVE, GST–EhFP4–CT), and two EhFP4 FL variants with a single (Cys375Ser) mutation or double (His365Ser/His366Ser) mutations in the FYVE domain were examined for their binding to various phospholipids. TF was used as a control. Abbreviations are: LPA, lysophosphatidic acid; LPC, lysophosphocholine; PtdIns, phosphatidylinositol; PtdIns(3)P, phosphatidylinositol-3-phosphate; PtdIns(4)P, phosphatidylinositol-4-phosphate; PtdIns(5)P, phosphatidylinositol-5-phosphate; PE, phosphatidylethanolamine; PC, phosphatidylcholine; S1P, sphingosine-1-phosphate; PA, phosphatidic acid; PS, phosphatidylserine.
C. Localization of EhFP4FL Cys375Ser mutant during phagocytosis. The trophozoites expressing HA-tagged EhFP4FL with the Cys375Ser mutation (HA–EhFP4FLCS) were co-cultured with Cell tracker blue-loaded CHO cells for 30 min, fixed and incubated with anti-HA and Alexa-488 conjugated antibody. The cells were then reacted with anti-mouse IgG antibody. (a–d) steady state; (e–h) phagosomes; (i–p) the phagocytic cup and the tunnel-like structure. Arrows indicate the HA–EhFP4FLCS-associated phagocytic cup. Bars, 10 m.

(2001) reported that PtdIns(3)P is recruited to the phagosomal membrane by *de novo* synthesis of PtdIns(3)P on the phagosome membrane, direct fusion and 'kiss and run' of the PtdIns(3)P-associated vesicles. Our results support that the 'kiss and run' mode of the PtdIns(3)P recruitment is dominant particularly in 'fast phagocytosis'. As shown in Fig. 1C (20 and 40 s, in particular), it was frequently observed that PtdIns(3)P vesicles were

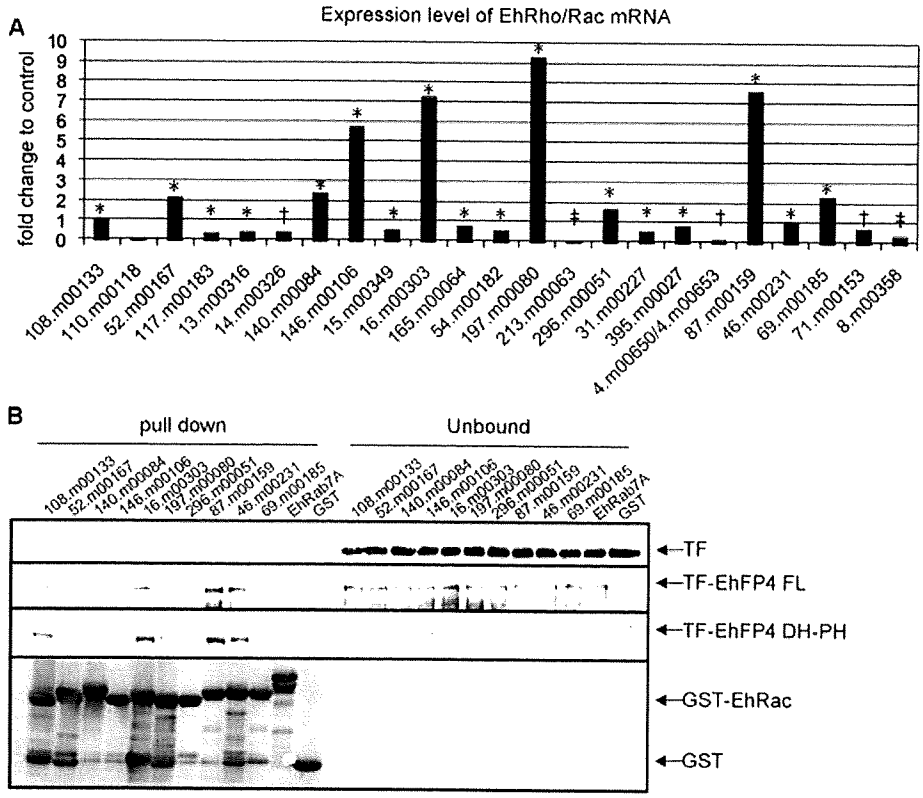

Fig. 5. Expression of *E. histolytica* Rho/Rac small GTPase genes and *in vitro* binding of EhFP4 to recombinant Rho/Rac.
A. The relative mRNA levels of putative Rho/Rac genes to RNA polymerase II is shown, based on a transcriptome analysis using DNA microarray. Detection *P*-value: $^{*}P < 0.00022$, $^{\dagger}P < 0.001$, $^{\ddagger}P < 0.01$.
B. Specific binding of EhFP4 to limited members of Rho/Rac. Glutathione-Sepharose resin bound to 1 of 10 GST–Rho/Rac, GST–Rab7A, or GST was incubated with TF–EhFP4FL, TF–EhFP4DH–PH or TF. After the unbound ('unbound') protein was collected, the resin was extensively washed, and the bound proteins were dissociated from the resin by incubating the resin with SDS-PAGE sample buffer ('pull down'). The 'unbound' and 'pull down' fractions were subjected to SDS-PAGE and immunoblot with anti-His (top three panels) or anti-GST antibody (bottom).

concentrated, accumulated around, and most of them were associated with the phagosome without fusing with the phagocytic cup and phagosome. It was also notable that a dramatic increase in the GFP–Hrs–FYVE signal occurred (Video S1, 1.483 min) soon after the primary phagosome came in contact with another preformed PtdIns(3)P-associated phagosome (0.824 min), but without direct fusion. These observations are consistent with the 'kiss and run' model. However, we could not exclude the possibility that the direct fusion of GFP–Hrs–FYVE-positive vesicles to phagosomes was underestimated because the direct fusion may have occurred too fast to be detected with the imaging system used in the present study. Furthermore, EhVps34, a type III phosphatidylinositol 3-kinase, was detected in phagosomes by proteomics studies (Marion *et al.*, 2005; Okada *et al.*, 2006). Thus, it is conceivable that synthesis of PtdIns(3)P by Vps34 on the phagosomal membrane could also be a source of PtdIns(3)P.

Significance of the intervesicle PtdIns(3)P-associated thread-like structures

We occasionally observed that PtdIns(3)P-associated phagosomes were continuously connected with other GFP–Hrs–FYVE-associated vesicles/vacuoles via the thread-like structures. These thread-like structures may mediate a bulk transfer of PtdIns(3)P from large PtdIns(3)P-positive vacuoles. Since these PtdIns(3)P-associated thread-like structures were often found to connect 'primary' and 'secondary' phagosomes (e.g. Video S2, 3.0 and 3.5 min), they may also serve to efficiently transport membrane and luminal materials necessary for the degradation of the content. Since these PtdIns(3)P-associated thread-like structures were rarely observed in the quiescent stage, their emergence is linked to the activation of PtdIns signalling associated with phagocytosis. Similar structures were reported in mammalian macrophages and *Caenorhabditis elegans* phagocytes (Ellson